Helsinki University of Technology
Department of Biomedical Engineering and Computational Science Publications
Teknillisen korkeakoulun Lääketieteellisen tekniikan ja laskennallisen tieteen laitoksen julkaisuja
Espoo 2010 REPORT A25

DYNAMICS OF SINGLE BIOPOLYMER TRANSLOCATION AND SEDIMENTATION

Ville Lehtola

Dissertation for the degree of Doctor of Science in Technology to be presented with due permission of the Faculty of Information and Natural Sciences for public examination and debate in auditorium F239a at Aalto University, School of Science and Technology (Espoo, Finland) on December 17th, 2010, at 12 noon.

Aalto University
School of Science and Technology
Department of Biomedical Engineering and Computational Science

Aalto-yliopisto
Teknillinen korkeakoulu
Lääketieteellisen tekniikan ja laskennallisen tieteen laitos

Distribution:
Aalto University
Department of Biomedical Engineering and Computational Science
P.O.Box 12200
FI-00076 AALTO
FINLAND

Tel. +358 9 470 23172
Fax +358 9 470 23182
http://www.becs.tkk.fi

http://lib.tkk.fi/Diss/2010/isbn9789526035109

ISBN 978-952-60-3509-3 (printed)
ISBN 978-952-60-3510-9 (pdf)
ISSN 1797-3996

Picaset Oy
Helsinki 2010

Aalto University

ABSTRACT OF DOCTORAL DISSERTATION	AALTO UNIVERSITY SCHOOL OF SCIENCE AND TECHNOLOGY P.O. BOX 11000, FI-00076 AALTO http://www.aalto.fi

Author Ville Lehtola

Name of the dissertation

Dynamics of single biopolymer translocation and sedimentation

Manuscript submitted 22.9.2010	Manuscript revised 22.11.2010

Date of the defence 17.12.2010

☐ Monograph ☒ Article dissertation (summary + original articles)

Faculty	Faculty of Information and Natural Sciences
Department	Department of Biomedical Engineering and Computational Science
Field of research	Biological physics, Statistical physics
Opponent(s)	Davide Marenduzzo, PhD
Supervisor	Prof. Kimmo Kaski
Instructor	Riku Linna, PhD

Abstract

In this Thesis the dynamics of translocation and sedimentation of a single biopolymer (typically DNA, RNA or a protein) is studied. A coarse–graining paradigm is invoked to justify the various computational models by use of which the results are obtained.

The transport of biopolymers through a nano-scale pore in a membrane is a ubiquitous process in biology. Experimental interest in translocation process focuses on its potential applicability in ultra-fast sequencing of DNA and RNA molecules. Polymer translocation has been under intense study for over a decade. Inspite of the vast theoretical research, the experimental results on the driven case have not been explained. We claim that the reason for this is that the translocation process must be treated as (at least) two dynamically distinct cases, where the dynamics takes place either close to or out of equilibrium. Here, we find that the latter case corresponds to the experiments. We make a comprehensive investigation on how the process can be discriminated based on its dynamics, and define and use some indicators to this end. In addition, we study the role of hydrodynamics, and find it to govern the dynamics when the process takes place out of equilibrium.

Sedimentation is a natural process induced by gravity that can be applied experimentally in a quickened form by the use of ultracentrifuges, and which is similar to electrophoresis. Our study on behavior of single polymers under non-equilibrium conditions falls within the rapidly developing field of nano- and microfluidics that has important applications in ''lab-on-a-chip" based technologies. In polymer sedimentation, we study the settling of the polymer in a steady-state in the limit of zero Péclet number, i.e. where no thermal fluctuations exist. The hydrodynamic coupling of the polymer beads leads to chaotic time-dependent behavior of the chain conformations that in turn are coupled with the velocity fluctuations of the polymer's center of mass.

Keywords polymer, translocation, dynamics, equilibrium, non-equilibrium, rheology, sedimentation

ISBN (printed) 978-952-60-3509-3	ISSN (printed) 1797-3996
ISBN (pdf) 978-952-60-3510-9	ISSN (pdf)
Language English	Number of pages 69

Publisher Department of Biomedical Engineering and Computational Science

Print distribution Department of Biomedical Engineering and Computational Science

☒ The dissertation can be read at http://lib.tkk.fi/Diss/2010/isbn9789526035109

Aalto-yliopisto

VÄITÖSKIRJAN TIIVISTELMÄ	AALTO-YLIOPISTO TEKNILLINEN KORKEAKOULU PL 11000, 00076 AALTO http://www.aalto.fi

Tekijä Ville Lehtola

Väitöskirjan nimi

Biopolymeerin dynamiikka translokaatiossa ja sedimentaatiossa

Käsikirjoituksen päivämäärä 22.9.2010	Korjatun käsikirjoituksen päivämäärä 22.11.2010
Väitöstilaisuuden ajankohta 17.12.2010	
☐ Monografia	☒ Yhdistelmäväitöskirja (yhteenveto + erillisartikkelit)

Tiedekunta	Informaatio- ja luonnontieteiden tiedekunta
Laitos	Lääketieteellisen tekniikan ja laskennallisen tieteen laitos
Tutkimusala	Biologinen fysiikka, Statistinen fysiikka
Vastaväittäjä(t)	Davide Marenduzzo, PhD
Työn valvoja	Prof. Kimmo Kaski
Työn ohjaaja	Riku Linna, FT

Tiivistelmä

Tässä väitöskirjassa tutkitaan biopolymeerin (tyypillisesti DNA, RNA tai proteiini) translokaatiota ja sedimentaatiota. Tutkimusparadigmana käytetään *coarse–graining* periaatetta ja tulokset saadaan eri malleilla tehdyistä tietokonesimulaatioista.

Translokaatio eli biopolymeerien siirtyminen membraanissa olevan pienen raon läpi on yleinen prosessi biologisissa systeemeissä. Translokaatioprosessin tavoiteltu kokeellinen sovellus on ultra-nopea DNA- ja RNA-molekyylien sekvenssointi, joka mahdollistaisi mm. räätälöidyt lääketieteelliset hoidot. Polymeerin translokaatiota on tutkittu intensiivisesti yli kymmenen vuoden ajan, mutta laajasta teoreettisesta työstä huolimatta ajettuun tapaukseen liittyviä kokeellisia tuloksia ei ole pystytty selittämään. Ajetussa translokaatiossa polymeeri siirtyy raon läpi ionivuon muodostaman sähköisen voiman avulla. Prosessi voidaan jakaa (ainakin) kahteen dynaamisesti erilaiseen tapaukseen ajavan voiman suuruuden mukaan: se etenee joko lähellä tai kaukana termistä tasapainoa. Tässä työssä nämä kaksi tapausta käsitellään erikseen ja tehdään vertaileva selvitys niiden erottamiseen tarvittavista indikaattoreista. Lisäksi tutkitaan hydrodynamiikan roolia prosessin aikana, joka osoittautuu dynaamisesti määrääväksi kaukana termisestä tasapainosta tapahtuvassa translokaatiossa.

Sedimentaatio on gravitaation aikaansaama luonnollinen prosessi, jota voidaan ultrasentrifuugilla kokeellisesti hyödyntää nopeutetussa muodossa. Prosessina se on samankaltainen kuin elektroforeesi. Tässä työssä tehty tutkimus on kiinteä jatke nopeasti kehittyvään nano- ja mikrofluidistiikan tutkimukseen, jonka yksi tärkeä sovellutus on “lab-on-a-chip”- pohjainen teknologia. Sedimentoituvaa polymeeria tutkitaan seuraamalla sen liikkeitä ja sen sisäistä konformaatiota. Polymeeriketjun keskimääräinen massakeskipisteen nopeus ja konformaatiota kuvaava gyraatiosäde ovat ajan suhteen muuttumattomia liikkeen aikana, eli vallitsee ns. *steady-state*. Hydrodynaamiset vuorovaikutukset ketjun eri osien välillä johtavat sisäisen konformaation ja siihen kytköksissä olevan massakeskipisteen nopeuden kaoottiseen aikakäyttäytymiseen. Sedimentaatiosimulaatioissa ei otettu huomioon termisiä vuorovaikutuksia, eli Péclet:in luku on nolla.

Asiasanat polymeeri, translokaatio, dynamiikka, tasapaino, epätasapaino, sedimentaatio

ISBN (painettu) 978-952-60-3509-3	ISSN (painettu) 1797-3996
ISBN (pdf) 978-952-60-3510-9	ISSN (pdf)
Kieli Englanti	Sivumäärä 69

Julkaisija Lääketieteellisen tekniikan ja laskennallisen tieteen laitos

Painetun väitöskirjan jakelu Lääketieteellisen tekniikan ja laskennallisen tieteen laitos

☒ Luettavissa verkossa osoitteessa http://lib.tkk.fi/Diss/2010/isbn9789526035109

Preface

The work for this Thesis was carried out while I was working at the former Helsinki University of Technology, now known as Aalto University. I started in the Computational Nanoscience (COMP, Academy of Finland Center of Excellence) group (Article V) and ended up in the Department of Biomedical Engineering and Computational Science (BECS, Centre of Excellence in Computational Complex Systems Research chosen by the Academy of Finland for 2006-2011).

I wish to thank my instructor PhD Riku Linna for the opportunity to work with him, and for showing me that science, at its best, follows from an individual's strive to grow his understanding. I wish to thank my supervisor Professor Kimmo Kaski, who has been good in facilitating the work, and providing suitable working conditions to do science. I also want to thank my collaborators of Article V, PhD Olli Punkkinen and Professor Tapio Ala-Nissilä, and finally my colleagues at work for interesting discussions during coffee breaks and others.

During the four years work at many hypotheses were tested. Reflecting on the past, some of them turned out to be right and some wrong, but they usually set a path to follow — even if it initially lead in an odd direction. The road was not always an easy one. In particular, the ineffectivity of the Finnish healthcare system extended my sick leave in 2009 by several months to the point where I had to rely on (expensive) private care to have my shoulder operated.

As a natural scientist, I believe that all problems in life can be solved. However, the humanist inside me says that everything doesn't have to be problematized. Most importantly, this guideline has provided me a smooth and loving relationship with my wife Terhi, who I wish to thank for sharing the same natural–scientist–mindset with me. And my dear family, thank you.

This work, as a requirement for the dissertation, is a demonstration of both my ability to think analytically and to write scientific text. I feel it to be my application to join the scientific community that consists of many great minds of the humanity. This is my thesis.

In Espoo, 16th of November 2010

Ville Lehtola

Contents

Errata

List of Publications

This thesis consists of an overview and of the following publications which are referred to in the text by their Roman numerals. In the overview, the Publications are referred to as Articles.

I Dynamics of forced biopolymer translocation,
V. V. Lehtola, R. P. Linna and K. Kaski - EPL 85, 58006 (2009)

II Critical evaluation of the computational methods used in the forced polymer translocation, V. V. Lehtola, R. P. Linna, and K. Kaski - Phys. Rev. E 78, 061803 (2008)

III Unforced polymer translocation compared to the forced case,
V. V. Lehtola, R. P. Linna, and K. Kaski - Phys. Rev. E 81, 031803 (2010)

IV Pore-polymer interaction reveals non-universality in forced polymer translocation, V. V. Lehtola, K. Kaski, and R. P. Linna - Phys. Rev. E 82, 031908 (2010)

V Polymer scaling and dynamics in steady-state sedimentation at infinite Péclet number, V. Lehtola, O. Punkkinen, T. Ala-Nissila - Phys. Rev. E, 76, 051802, (2007)

Author's contribution

The author has played an active role in all stages of the research reported in this Thesis.

Publications I-IV were coauthored with Dr. Riku Linna and Professor Kimmo Kaski. The author wrote the first drafts of the articles. A substantial part of the writing of the articles to bring them to their final form and substance was done by Riku Linna. The author performed all computational work involved. He participated actively in the development of concepts and ideas on which the articles were based on.

Publication V was coauthored with PhD Olli Punkkinen and Professor Tapio Ala-Nissilä. The author did all the computational work. He participated actively in the development of concepts and ideas, and wrote the first draft of the paper, excluding the introduction and the theoretical model.

List of Abbreviations

In alphabetical order.

DNA	Deoxyribonucleic Acid
DP	Degree of Polymerization
ds	double stranded (e.g. dsDNA)
FJC	Freely Jointed Chain
IB	Immersed Boundary (method)
LD	Langevin Dynamics
MD	Molecular Dynamics
MC	Monte Carlo (method)
RNA	Ribonucleic Acid
SRD	Stochastic Rotation Dynamics
ss	single stranded (e.g. ssDNA)
WLC	Worm-Like Chain
3D	3 dimensions (also 1D, 2D etc.)

List of Symbols

In order of appearence. Bolded symbols represent vectors.

x	length of a spring
b	average bond length between two monomers, Kuhn length
M	total mass of a polymer chain
m	mass of one bead
N	length of a polymer chain in monomer units
U_{FENE}	finitely extensible nonlinear elastic potential
K	coefficient of the FENE potential
R	maximum bond length
r	distance between two beads
$\mathbf{r}_i$	location of monomer i, $i \in [1, N]$
σ	length unit used in monomer pair-potentials (also stress tensor in Chapter 4)
ϵ	energy quantity of Lennard-Jones potential
U_{LJ}	Lennard-Jones potential
$\mathbf{R}_{ee}$	end-to-end vector
$\mathbf{R}_n$	segment-to-segment vector
U	potential
U_p	potential perpendicular to the pore axis inside the cylinder pore
k_p	spring constant
C_p	damping constant
$\mathbf{p}_i$	momentum of bead i
β	$= 1/k_B T$ (also scaling exponent in translocation problem)
k_B	Boltzmann's constant (computational constant is k)
T	temperature
Z	partition function
$\psi(\mathbf{p}_n, \mathbf{r}_n)$	probability distribution function

R_G	radius of gyration
C	constant
ν	swelling exponent (also kinematic viscosity in Chapter 4)
t	time
$\dot{\mathbf{r}}_i$	time derivative of the location (here: velocity) of bead i
∇	gradient
$\nabla\cdot$	divergence
γ	surface critical exponent
$R(t)$	a Gaussian process
$\delta(t)$	Dirac delta function
H	drift
D	diffusion coefficient
μ	connective constant
d	dimension
F	Helmholtz free energy
s	reaction coordinate
S	entropy
$\Delta\mu$	chemical potential
$P(x,t)$	probability density
ξ	friction
J	probability density current
R_{kr}	Kramers escape rate
E_c	energy
ρ	fluid density
$\mathbf{u}$	fluid velocity
$\mathbf{f}$	force
Re	Reynold's number
η	viscosity
L	length (may be characteristic)
V	characteristic velocity

g	strength of a gravitational field
$\Delta\rho$	buoyant density
ρ_p	mass density of a particle
a	hydrodynamical radius of a particle
Pe	Peclet number
ζ	coefficient of the viscous drag
α	rotation angle in Chapter 4, scaling exponent in Chapter 5
$\underline{\mathbf{R}}$	SRD rotation matrix
Q	amount of fluid particles in simulation
f_{tot}	total external driving force experienced by the polymer, so-called total pore force
q	electric charge
$P_f(s)$	forward transition probability (towards trans side)
τ	average translocation time
$\pi(\tau)$	distribution of translocation times
R_{pe}	bead to pore distance
$\mathbf{v}_{cm}$	velocity of the center of mass
$\mathbf{v}_{cm,\perp}$	$\mathbf{v}_{cm}$ perpendicular to the flow
$\mathbf{v}_{cm,\parallel}$	$\mathbf{v}_{cm}$ parallel to the flow
v_{lim}	steady-state settling velocity
$\delta\mathbf{v}$	velocity fluctuation, from v_{lim}
k	spring constant
c	concentration of monomers per volume

List of Figures

List of Tables

1 Introduction

Nature has been the inspiration of philosophers and natural scientists since the dawn of Western philosophy. We are surrounded by the abundance of complex natural phenomena. To deal with this complexity, we choose a coarse-graining approach [66] that is common in natural and crucial in computational science[1]. It enables us to neglect a multitude of insignificant details, and study the essential components of these phenomena. Hence, it enables the use of tools of our respectful field of science for analysis.

In this thesis, two natural phenomena, polymer translocation and polymer sedimentation, are studied with the means of computational and statistical physics. This text has been written as a part of the requirements for doctoral dissertation and, as such, meant to be read by fellow physicists.

The aim of the coarse-graining used in this work is not to discover fundamentals (or pieces of puzzle) that could be assembled in a constructionistic way to acquire the original system (or puzzle), but instead discover the inherent properties that are characteristic to the system. This philosophical point of view is explained by Anderson [5], who sees physics, in general, as a study of symmetries. This idea of symmetries, and symmetry breaks (such as phase transitions), appearing on different scales of abstraction is close to previously introduced *General System Theory* by von Bertalanffy [84] as being a paradigm for development of theories. In polymer translocation, it is easy to see that the system symmetry plays a role, considering for example the 'eternal struggle' of the external and the inherent entropic forces of the system. We can ask: at what point does the equilibrium framework break down when the force is increased? Do the long chains exhibit different behavior, some kind of 'long range symmetry breaking', from the short ones?

The text is written using inclusively the pronoun 'we'. With this the writer flexibly refers

[1] For the role of coarse-graining in the metaphysics of causation, see e.g. [74].

to various groups of people. Typically the pronoun refers to the members of the research group with whom the article related to the subject at hand was made. However, at some points the pronoun can be thought to consist of the writer and the reader. Finally, this choice was motivated to pronounce the cooperative interaction of the people that leads to scientific excellence.

This text introduces and summarizes the study that has been done in the attached articles, and proceeds as follows. In the first Chapter, the phenomena, polymer translocation and polymer sedimentation, and literature concerning them, are introduced. In the second Chapter, the phenomena are treated as systems, which can be coarse-grained into a model of a single polymer that is computationally tractable and mathematically sound. The inherent solvents of these systems are excluded at this point and explained in Chapter 4. In the third Chapter, the concepts for analysis for the previously introduced models are presented. In the fourth Chapter, the solvent is treated in different frameworks. In the fifth Chapter, the results of this work are presented, meaning that the analysis of the phenomena is made using the introduced concepts. Finally, in the sixth Chapter, the conclusions of the work are drawn. The reader should be aware that the subjects in this text are presented rather in a pedagogical order than a chronological one based on the order that the papers were published.

Let us begin by introducing the concept of a polymer.

1.1 Polymers and biopolymers

Polymers are molecules subject to complex intra- and intermolecular interactions combined with many intramolecular degrees of motional freedom. The word ‘polymer’ originates from Greek, and literally means ‘many parts’. In fact, polymers are made up of monomer repeat units. The degree of polymerization (DP), which ranges typically from 10^2 to 10^6, denotes the number of monomer units jointed together in a polymer. Natural

polymeric materials consist of fossilic fuels, cellulose, amber, and rubber. Plastics contain a lot of different synthetic polymers, PVC for example. Other synthetic polymers also exist, for example, nylon and kevlar. Polymers are also abundant in biological systems. This subclass of polymers is referred to as biopolymers, and consists, for example, of DNA, RNA, and proteins. Biopolymers are typically electrically charged, which is an important property related to many biological phenomena. Because of the wide applicability, it is not surprising that the study of polymers in different contexts has been, and still is, intense.

A polymer can have various types of configurations, of which the three basic ones include linear, branched, and network (cross-linked chains) configurations. In addition to weight, DP and configuration properties, the morphology of the polymer is also an important property and for example greatly influences the properties of thermoplastics. The polymer morphology contains three basic classifications: amorphous, semi-crystalline and crystalline. In this thesis, the attention is limited on amorphous linear chains, referred to as 'polymers' for simplicity.

1.2 Polymer translocation

Sanger received a Nobel price in 1959 for a research work that showed, for the first time, that proteins are composed of linear polypeptides formed by joining amino acid recidues in a defined, but apparently arbitrary order [71, 72]. The idea of a linear information sequence was quickly adapted for DNA, leading to the first DNA sequencing experiment to take place in 1968, and the discovery of the modern gel-based DNA sequencing method in 1977 [34]. The new method was used later-on in automated sequencing factories hastening the completion of the Human Genome Project that was concluded in 2003. Many spinoff projects[2] were launched during and after the Human Genome Project. Hopes for a new ultra-fast sequencing were lifted when Kasianowicz et al. [37]

[2]http://www.ornl.gov/sci/techresources/Human_Genome/research/spinoffs.shtml

showed that measurements of the ionic current flowing through nanometer-scale pores (nanopores) could be used to analyze single DNA and RNA molecules. Experimental work on this so-called *forced polymer translocation* has been typically conducted by using fabricated solid-state [79, 46] pores or α-hemolysin ($\alpha-$HL) pores in lipid bi-layer membranes [56, 37]. Attempts at purely electronic measurements had trouble achieving the signal contrast required for single nucleotide differentiation until 2007 [77]. A multitude of theoretical and computational papers have been published since the start of the ultra-fast translocation boom in 1996 (see Refs. of Articles I-IV).

In biology, the transport of biopolymers, such as DNA, RNA and proteins, through a nano-scale pore in a membrane is a ubiquitous process. Similarities with the experimental forced polymer translocation exist. For example, in protein import into different cell compartments, such as mitochondria, chloroplasts, and peroxisomes the translocation occurs with the aid of a membrane potential [1]. One of the key questions has been, whether the natural process is possible without any other mechanisms than the eletrophoresis [83]. In Fig. 1.1, protein import into mitochondrion is depicted[3].

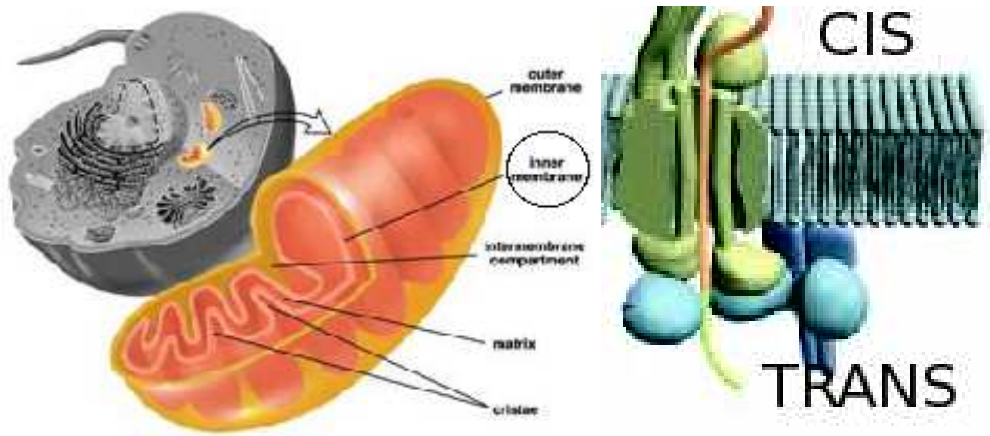

Figure 1.1: An example of polymer translocation. Left: a mitochondrion inside a cell. The text inner membrane is encircled. Right: a lipid bilayer with a translocase. A protein that is translocating into the *trans* side, is represented by a yellow tube with a green front. The words trans and cis come from the word transis.

[3]Left figure is from http://kconline.kaskaskia.edu/bcambron/Biology%20117/Cells.htm

Many transport processes function without the biopolymer being strongly electrophoresed, i.e. driven by a force, which has increased the interest on unforced polymer translocation [76]. Partly due to the the abundance of detailed processes adding to the complexity of its dynamics, such as binding of specific proteins on either the *cis* or *trans* side of the membrane, and the effects due to the properties of the pore and the solvent, experimental studies on unforced translocation are few [6] compared with the abundance of available computational studies, see *e.g.* [15, 47, 33, 22, 61, 31, 3, 28]. Another reason for the abundance of computational studies is the paradoxal nature of the polymer translocation problem. On one hand, it seems like a well-defined statistical-mechanical problem, where familiar concepts of criticality such as universality can be applied. On the other hand, it is a problem consisting of non-linearities such as anomalous diffusion and many-particle hydrodynamics. The problem is interesting for statistical physicists, and the non-linearities provide a suitable need for computational research. However, polymer translocation is, most importantly, a transport problem that, by definition, deals with finite size effects that render the assumptions used for criticality questionable. The paradox of the problem that exists between apparent criticality, and the finite size gives a conceptual challenge in setting frames for this Thesis.

How these two processes, forced and unforced translocation, differ conceptually and otherwise, will be discussed in Chapter 3. However, it is noteworthy to point out that both of these mechanisms are relevant, for example, in the protein import mechanism into mitochondria, which has been under intense study for almost two decades, see e.g. [85, 58] and references there-in. The phenomena can be split into two processes, transits through the outer and inner membrane, of which only the latter has an electrical potential over it.

1.3 Polymer sedimentation

Sedimentation is a natural phenomenon induced by gravity, see Fig. 1.2. The process is applied experimentally in a quickened form by the use of ultracentrifuges. Two different

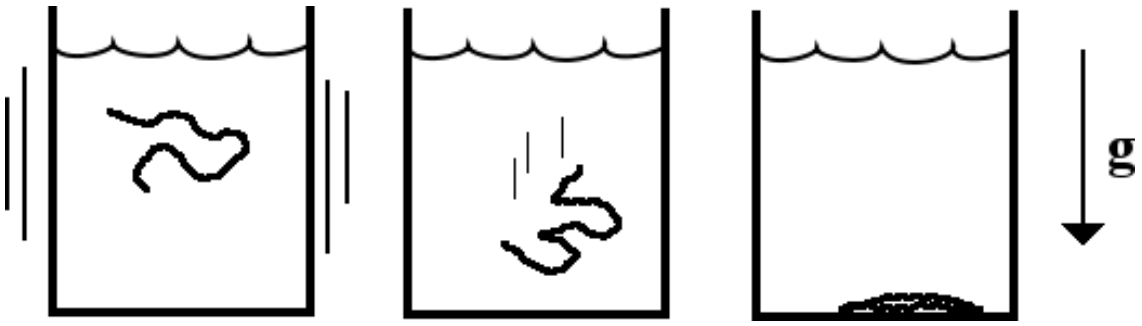

Figure 1.2: A cartoon depicting polymer sedimentation. Left: A solvent including an added polymer is shaken. Center: The gravity **g** acting upon the polymer makes it sedimentate towards to bottom. The different parts of the polymer interact via the complex fluid field that they exhibit. Right: The sedimentation process is ended as the polymer reaches the bottom.

kinds of experiments are commonly performed on these instruments: sedimentation equilibrium experiments and sedimentation velocity experiments. The first kind is concerned only with the final steady-state of the experiment, where sedimentation is balanced by diffusion opposing the concentration gradients, resulting in a time-independent concentration profile. The experiment then describes the final stage of the process that corresponds to the rightmost frame in Fig. 1.2. Unlike in the figure, centrifuge experiments typically consist of multiple polymers. The second kind, like the simulations done for this Thesis, aims to interpret the time-course of sedimentation, which is illustrated by the middle frame of Fig. 1.2. Typical quantities of interest are the shape and molar mass of the dissolved macromolecules, as well as their size-distribution.

The rheological properties of polymer melts and solutions have been under intense study for many decades due to their non-Newtonian hydrodynamic behavior and important applications in materials processing [10]. With the rapidly developing field of nano- and microfluidics [59, 78], and their important application in “lab-on-a-chip” based technologies, it has become crucial to understand the behavior of single polymers under non-equilibrium conditions. In electrophoresis, which is a process similar to sedimentation, hydrodynamic shielding has been found important even at the oligomer range of poly-

electrolyte chains, to produce correct dynamics [29].

2 Coarse-graining of molecular structures

In order to study the presented phenomena of polymer translocation and polymer sedimentation, we coarse-grain the molecular structures.

2.1 From macromolecules into polymers

The basic idea behind coarse-graining is that any kind of long linear molecule, which can even consist of about 10^8 atoms (DNA) and different kinds of bonds, can be described by fewer degrees of freedom depending of the details of the model. Using a coarse-grained model, and comparing its behavior to the experimental results, it can be verified that all the crucial mechanisms have been included in the model. When the underlying mechanisms are revealed, the parametric model can describe all polymers satisfying the assumptions of the respective model. Coarse-graining is indeed needed, since the computationally feasible amount of degrees of freedom, for our polymers, is of the order of 10^3 or 10^4. An example of polymer coarse-graining is demonstrated in Fig. 2.1.

The length scale of polymers ranges from the order of nanometers up to the order of micrometers. Thus the study of polymers incorporates concepts of classical physics such as elasticity. In our study, where we ignore bending potentials, the primary quantity describing our model polymers is length, which is discretized into (homogenous) repeat units, and the molecular structure is approximated by beads with mass and massless springs, see Fig. 2.1. Here we note that the monomers of the coarse-grained model polymer (i.e. beads) are different from the monomers of the macromolecule. The amount of beads, or (computational) monomers, N adequately describes the contour length of the polymer, when multiplied with the average spring (or bond) length b. The length b is determined from the elastic properties of a real polymer, i.e. how the polymer responds to bending or

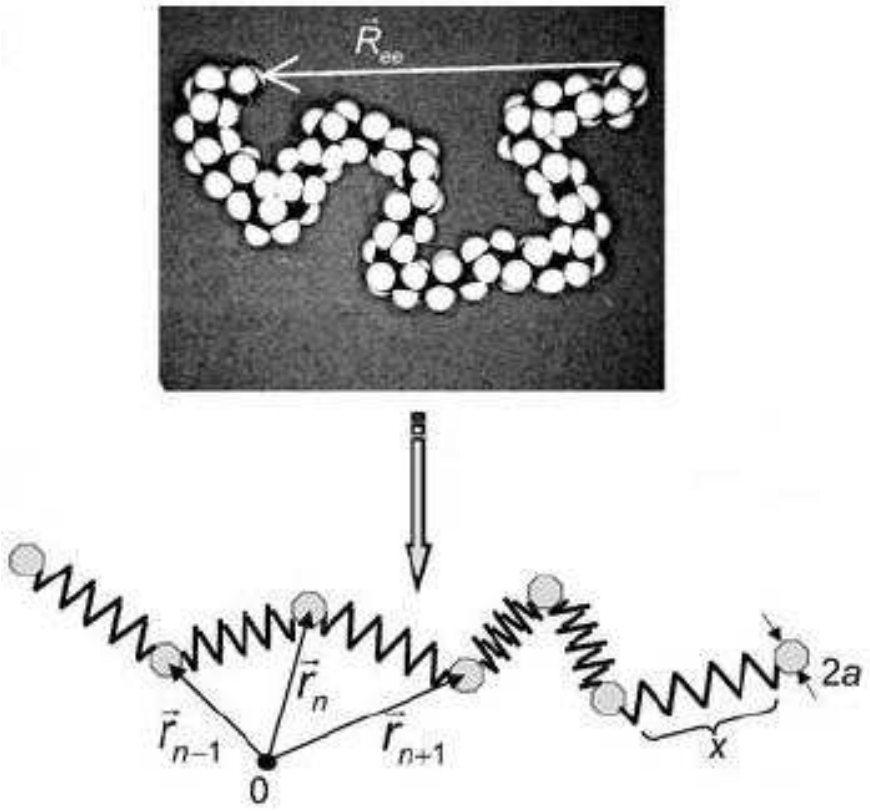

Figure 2.1: A polymer (upper figure) is coarse-grained into Kuhn segments (lower figure). The beads represent the mass of the segments, and are labelled from 1 to N. The figure is from Ref. [39]. The repeat units, i.e. monomers, of the coarse-grained model polymer are different from the monomers of the macromolecule. The former are also referred to as beads.

twisting

$$b \equiv \sqrt{\langle x^2 \rangle} \tag{2.1}$$

of the lengths x of the springs, see Fig. 2.1. The magnitude of b depends on the choice made for the potential used for springs. In this thesis, the classical concept of Kuhn length is used. For a real polymer, the length of a Kuhn segment is taken just large enough to permit ignoring any stereochemical restriction of the orientation of the Kuhn segments relative to each other. In the polymer model, two adjacent particles or beads are thus connected by a one-dimensional potential (i.e. the spring) that is dependent on the

distance between the beads. No mutual orientation correlation exists between the beads. The conformational statistics of such a freely jointed chain (FJC) of N, where $N \gg 1$, Kuhn segments is mathematically equivalent to a random walk. This changes if a self-avoiding potential is included, although in the following it is still called a freely jointed chain.

2.2 Freely jointed chain

The bead-spring chain, used as a coarse-grained polymer model, is computationally modeled as point-like particles at coordinates $\{\mathbf{r}_1, \mathbf{r}_2, \ldots, \mathbf{r}_N\}$ that are connected by springs. Unlike the springs, the particles have a mass m. The total mass of the chain M is then proportional to the degree of polymerization, or the amount of monomers, $M \sim N$. Adjacent monomers are connected with anharmonic springs that are described by the finitely extensible nonlinear elastic (FENE) potential,

$$U_{\text{FENE}} = -\frac{K}{2} R^2 \ln\left(1 - \frac{r^2}{R^2}\right), \tag{2.2}$$

where $r = |\mathbf{r}_i - \mathbf{r}_j|$ is the length of an effective bond between beads i and j and $R = 1.5$ is the maximum bond length in our simulation units. The Lennard-Jones (LJ) potential

$$\begin{aligned} U_{\text{LJ}} &= 4\epsilon\left[\left(\frac{\sigma}{r}\right)^{12} - \left(\frac{\sigma}{r}\right)^{6}\right],\ r \leq 2^{1/6}\sigma \\ U_{\text{LJ}} &= 0,\ r > 2^{1/6}\sigma, \end{aligned} \tag{2.3}$$

is used between all beads of distance r apart. The parameter values were chosen as $\epsilon = 1.2$, $\sigma = 1.0 = b$ and $K = 60/\sigma^2$. The used LJ potential with no attractive part mimics good solvent, i.e. the particles are soluble to the solvent. The spring equations (2.2) and (2.3) contain only radial dependence, and thus describe a so-called *freely jointed chain* (FJC), which is used in all the Articles from I to V. A widely used model that extends the FJC model by including an angular dependence is called the worm-like chain (WLC) [4]. An additive ε term may be added to the potential of Eq. (2.3), though the

current form was also numerically stable and we obtained the correct swelling exponent $\nu = 0.60 \pm 0.02$ in 3D.

2.3 Radius of Gyration

A flexible chain, such as the FJC, goes through different configurations even in equilibrium. In the canonical ensemble, the contour length of the polymer $L = bN$ remains constant, even if its configuration changes. One way to characterize the conformation of the polymer is the end-to-end vector, which is written as

$$\mathbf{R}_{ee} = \sum_{n=1}^{N} \mathbf{R}_n. \tag{2.4}$$

Here, the segment-to-segment vector $\mathbf{R}_n \equiv \mathbf{r}_n - \mathbf{r}_{n-1}$. The Kuhn segments are defined as not having any rotational restrictions, and thus $\langle \mathbf{R}_n \rangle = 0$ for equilibrium random walk, where the brackets denote an average over the distribution function

$$\psi(\mathbf{p}_n, \mathbf{r}_n) = \frac{e^{-\beta\left[\frac{\mathbf{p}_n^2}{2m} + U(\{\mathbf{r}_n\})\right]}}{Z}. \tag{2.5}$$

Here, Z is the canonical partition function for the system, and is written as

$$Z = \prod_{n=1}^{N} \int d\mathbf{p}_n d\mathbf{r}_n \, e^{-\beta\left[\frac{\mathbf{p}_n^2}{2m} + U(\{\mathbf{r}_n\})\right]}. \tag{2.6}$$

Another way to represent the size (or shape) of the polymer is to use the mean squared radius of gyration [20]

$$R_G^2 = \frac{1}{N} \sum_{i}^{N} \langle (\mathbf{r}_i - \bar{\mathbf{r}})^2 \rangle, \tag{2.7}$$

where $\mathbf{r}_i$ is the location of the segment i and $\bar{\mathbf{r}} = \frac{1}{N} \sum \mathbf{r}_i$ is the location of the center of mass of the polymer. The advantage of R_G over $\mathbf{R}_{ee}$ is that it is well defined even for branched polymers, and it can be viewed as a value describing the radius of a sphere occupied by the polymer.

In equilibrium, the radius of gyration R_G and the end-to-end vector $\mathbf{R}_{ee}$ scale identically with respect to N [20]. We have a relation

$$\langle R_G^2 \rangle = C \langle \mathbf{R}_{ee}^2 \rangle \simeq (N^\nu b)^2, \tag{2.8}$$

where $\mathbf{R}_{ee}$ is defined by Eq. (2.4), and $C = 0.1599 \pm 0.0002$ in 3D [45]. The self-avoidance of the beads results in increased volume occupied by the polymer (in contrast to the ideal chain), and is described by the swelling exponent

$$\nu = \frac{\log(R_G)}{\log(N)}. \tag{2.9}$$

In equilibrium, the exponent is universal, depending only on the dimension. In $2D$ $\nu = 0.75$, while in $3D$ $\nu = 0.5888$, and it saturates to the mean-field exponent $\nu = 0.5$ in $4D$ and higher dimensions. Hence, dimension four is the upper critical dimension for self-avoiding random walk.

2.4 Bi-layers and pores as planes and potentials

In Articles I to IV, the lipid bilayer that contains the nanopore through which the polymer translocates is replaced by a mathematically defined plane. The pore model used by us in Articles I–III is a homogeneous cylinder, whereas others [50, 49, 27, 25] have used a wall of immobile (point-like) particles through which the pore is typically implemented by removing a single particle, see Fig. 2.2. These differ in, for example, that the latter implementation of the pore does not result in a potential that is homogeneous with respect to the direction of the translocation velocity . Other pore models include both square [25], and cylinder [8] shaped pores used in lattice Boltzmann simulations. Furthermore, computational pore-polymer interaction studies include extending the pore diameter and the LJ potential cutoff length in 2D so that an attractive potential between the polymer and pore beads forms in the middle of the pore [48].

In Article IV, we have conducted a comparison of the two most widely used pore models, the one made of immobile particles and our cylinder pore, see Fig. 2.2. The latter is more

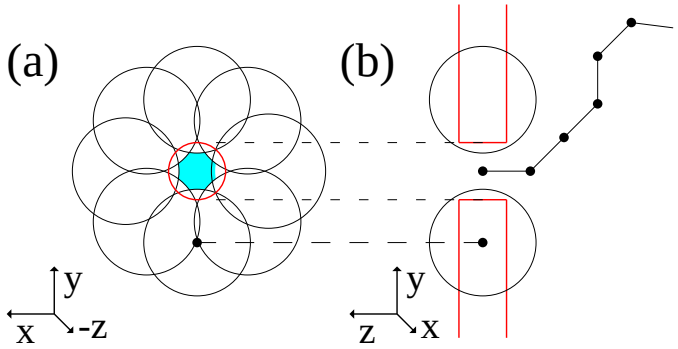

Figure 2.2: Schematic depiction of the two pore models. (a) The pores are viewed from the *trans* side along the z-axis. The small red circle depicts the cylindrical pore of diameter 1.2σ. The bead pore is defined by the eight beads each at distance 1.5σ from the z-axis. The pore beads are drawn with circles using the LJ potential cutoff length $2^{1/6}$ as their radius. The light blue area in the center of the pore indicates the region where polymer beads have no interaction with the pore beads. In contrast, the cylinder pore model has a damped-spring-like potential that acts on particles everywhere inside the pore. (b) Side view. The polymer about to translocate ($s = 1$) is drawn as connected dots. The potentials of the two pore models differ in both the xy-plane and along the z-axis.

aligned with the coarse-graining principle, being simpler and more minimalistic than its counterpart. The latter was used in Articles I–IV, and is especially convenient as a model since it can be easily generalized into $d \geq 2$ dimension. In Articles I and III where the stochastic rotation dynamics (SRD) model is used, the slit walls are also represented by mathematical planes.

The cylindrical nanopore has a diameter of $1.2\ \sigma$, where $\sigma = b$. The force f acting on the beads inside the nanopore is constant and local for the pore, which models well the experimental setups and biological systems, where solvents are good ionic conductors thus eliminating any potential gradients outside the pore. The polymer beads inside the pore are not coupled with hydrodynamic modes in any of our simulations. In the directions perpendicular to the cylindrical pore, beads inside the pore experience a damped harmonic potential U_p, described by

$$-\nabla U_p = f_h = -k_p r_{x,y} - C_p v_{x,y}, \tag{2.10}$$

where $k_p = 100$, $C_p = 1$, $r_{x,y}$ are the spring constant, the damping constant, and the

position of polymer bead with respect to the center axis of the cylindrical pore, respectively, and $v_{x,y}$ is the velocity component perpendicular to the pore walls. (In Article I $k_p = 1000$ and $C_p = 10$.) Thus U_p centers the polymer along the z-directional axis of the pore. The potential is chosen large, so no hairpin configuration can enter the pore as its width is effectively small. Hence, the polymer segment inside the pore remains rather straight. In the z direction, the polymer beads experience either zero or finite friction in the pore. The beads experience either a slip or a no-slip boundary condition, simulations with both have been conducted. The no-slip boundary condition for the solvent (in simulations where hydrodynamics was used) will be described in Chapter 4.

In Articles I–IV, the ionic current over the membrane, i.e. through the pore, is simulated as a homogenous force field that acts only upon particles that reside inside the pore. In Article V, gravity is simulated as a force field covering the whole system. The force field originating from the fluid properties, thermal motion, and the motion of solute particles is treated with different approaches that are explained in Chapters 3 and 4.

3 Concepts for analysis

After coarse-graining the polymer, we basically have a many-body system of N interacting particles. For these, we can write the equations of motion that we can use to computationally investigate the time development of the system. A straightforward way to implement dynamics for an N-particle system in a canonical ensemble is to include a heat bath.

3.1 Fokker-Planck equation

To treat an N-particle problem analytically, we can use the Fokker-Planck equation

$$\frac{\partial P(\{\mathbf{r}_N\},t)}{\partial t} = -\sum_{i=1}^{N} \frac{\partial}{\partial x_i} \left[H_i(\mathbf{r}_1,\ldots,\mathbf{r}_N) P(\{\mathbf{r}_N\},t)\right] + \sum_{i=1}^{N}\sum_{j=1}^{N} \frac{\partial^2}{\partial x_i\, \partial x_j} \left[D_{ij}(\mathbf{r}_1,\ldots,\mathbf{r}_N) P(\{\mathbf{r}_N\},t)\right], \tag{3.1}$$

which describes the time evolution of the probability density function $P(\{\mathbf{r}_N\},t)$ of the position of N particles. Here H is the drift vector and **D** the diffusion coefficient in tensor form. The former represents deterministic motion, while the latter results from the presence of a stochastic (Brownian) force.

3.2 Langevin dynamics

If we neglect the hydrodynamic interactions between the particles, it suffices to simulate the particles in a heat bath. One way to do so is to account for omitted degrees of freedom by the use of stochastic differential equations. One typical approach is called Langevin dynamics, which mimics the viscous aspect of the solvent, and it was used in Articles

II–IV to model polymer translocation, since it is a computationally convenient method to simulate the time development of the system. Specifically, our algorithm was the one formulated by Ermak [4].

Consider a system of N particles with masses m in coordinates $\{\mathbf{r}_1(t), \mathbf{r}_2(t), \ldots, \mathbf{r}_N(t)\}$. The time-development of such a system can be described by Langevin equations of the form

$$m\ddot{\mathbf{r}}_i = -\nabla U(\{\mathbf{r}_i\}) - \xi\dot{\mathbf{r}}_i + \sqrt{2\xi k_B T m}R(t)\,, \tag{3.2}$$

where $U(\{\mathbf{r}_i\})$ is the particle interaction potential, $k_B T$ is the Boltzmann constant times the temperature, and $R(t)$ is a delta-correlated stationary Gaussian process with zero mean that is preceded by a prefactor that satisfies the fluctuation-dissipation theorem [65]. Specifically, $R(t)$ is required to satisfy

$$\begin{aligned} \langle R(t)\rangle &= 0 \\ \langle R(t)R(t')\rangle &= \delta(t-t'), \end{aligned} \tag{3.3}$$

where δ is the Dirac delta function. As we can see, the equations of motion (3.2) include a time-dependent random variable that accounts for Brownian motion, and a friction term ξ that mimics the viscosity.

3.3 Diffusive motion

The Fokker-Planck equation, Eq. (3.1), is quite general. A more intuitive form can be achieved, for example, by considering a single particle in equilibrium. In equilibrium, which is the limit of strong friction $|\xi v| \gg |m\dot{v}|$ for Langevin dynamics, the drift term can be taken to be $H = 0$. Also, if the diffusion tensor $\mathbf{D}$ is isotropic and constant in time, we obtain a diffusion equation

$$\frac{\partial p(\mathbf{r},t)}{\partial t} = D\,\nabla^2 p(\mathbf{r},t), \tag{3.4}$$

where the diffusion coefficient D is a constant obtained from [65]

$$D = \frac{kT}{m\xi}. \tag{3.5}$$

Neglecting hydrodynamical effects, the diffusion coefficient for the center of mass of the polymer scales as $D_{cm} \sim N^{-1}$. This is referred to as Rouse diffusion. With Stokes' approximation, using the Oseen tensor for hydrodynamical interactions, $D_{cm} \sim N^{-\nu}$, yields Zimm diffusion [20].

The one particle diffusion coefficient can be obtained from simulations as

$$D = \frac{1}{d}\int_0^\infty dt \langle \mathbf{v}(0) \cdot \mathbf{v}(t) \rangle, \tag{3.6}$$

where d is the dimension of the system, and the brackets denote an average over the phase space, i.e. time and simulations, hence assuming ergodicity. Typically, the ergodicity condition is somewhat relaxed when, for example, Lennard-Jones particles are considered. Here the bracketed quantity $C_t \equiv \langle \mathbf{v}(0) \cdot \mathbf{v}(t) \rangle$ is called the velocity autocorrelation function, and the special case $C(t = 0)$ yields the familiar result of the equipartition theorem $\langle v^2 \rangle = dkT/m$. For a Brownian particle in equilibrium the information about the initial velocity decays exponentially [65]

$$\langle \mathbf{v}(t_2) \cdot \mathbf{v}(t_1) \rangle = \frac{kT}{m} \exp\left(-\frac{\xi}{m} |t_2 - t_1| \right). \tag{3.7}$$

In addition to being interesting fundamental physics, Eqs. (3.5), (3.6), (3.7) can be used (as tools) to test the validity of computational models in equilibrium. The analytically obtained value for D of Eq. (3.5) should match the computationally obtained value of Eq. (3.6). Also, any equilibrium computational model should yield the exponential decay of Eq. (3.7). These tools have been used to verify the models used for this Thesis. In addition, Eq. (3.6) can be used for various purposes even outside equilibrium. In article V, we determine an *effective* diffusion coefficient for the center of mass of the polymer that is a result of complex coupling of hydrodynamical modes in the absence of thermal motion.

The self-avoiding effects in the diffusive transport of a single polymer turn out to affect the characteristic length scale. The average time for a free polymer to diffuse its own

length in equilibrium is

$$\tau = \frac{R_G^2}{D} \sim N^{1+2\nu}, \tag{3.8}$$

since $R_G \sim N^\nu$, and $D \sim N^{-1}$ with Rouse dynamics. Eq. (3.8) provides a lower limit for the scaling of the transport time, also in polymer translocation [36]. In the limit of no excluded volume, the scaling of Eq. (3.8) would give $\tau \sim N^2$.

3.4 Single polymer chain in equilibrium framework

A system that is (or is assumed to be) in thermal equilibrium can be treated in the equilibrium framework. Based on the equiprobability of the states of the system, the idea is to write a partition function that keeps track merely of the amount of states. The system is then fully described, except for the time scale of diffusive dynamics or possible fluctuations. Even introducing small perturbations to the system is allowed, since by the fluctuation-dissipation theorem the system has a self-relaxing property that works to restore the equiprobability of the states.

Let us consider a free polymer with fixed number of monomers N, i.e. a canonical ensemble. Assuming Boltzmann weights for particles in a heat bath with a constant temperature T, we can write the partition function as

$$Z_N = \prod_{i=1}^{N} \int d\mathbf{p}_n d\mathbf{r}_n \exp\left(-\beta \sum_n \left[\frac{\mathbf{p}_n^2}{2m} + U(\{\mathbf{r}_n\}) \right] \right), \tag{3.9}$$

where $U(\{\mathbf{r}_n\})$ is a potential acting on the beads, and $\beta = 1/k_B T$. Typically, one can calculate Z_N from Eq. (3.9) for simple systems, such as the ideal gas, by direct integration. Unfortunately, if U contains self-excluding terms, like in our case, we cannot solve the location dependent integral in Eq. (3.9) directly. However, another approach is possible.

If we consider a random walk (that is an ideal chain for $N \gg 1$) in a d-dimensional

lattice, the partition function can be straightforwardly calculated as

$$Z_N = \mu^N, \tag{3.10}$$

where $\mu = 2d$ is the connective constant describing the degrees of freedom of each particle. The addition of exclusion effects (no overlap of particles) alters the effective dimension of the system. A correction term is added to the partition function of Eq. (3.10) so that

$$Z(N) = \mu^N N^{\gamma-1}, \tag{3.11}$$

and the value of μ is altered. Here, γ is the so-called surface critical exponent. For an ideal chain $\gamma = 1$, and Eqs. (3.10) and (3.11) are equivalent. The self-avoiding polymer chain was theoretically shown to yield the same universality as the self-avoiding random walk by de Gennes [19]. The value of the connective constant, which describes the degrees of freedom of a particle, is bounded from above by $\mu \leq 2d$ (ideal chain), and from below by $\mu \geq d$ (diffusion only towards positive axes). The limit value is defined as $\mu \equiv \lim_{N\to\infty} \mu_N$, where $\mu_N = c_d^{1/N}$, and the value of c_d is the lattice self-avoiding walk (SAW) enumeration [51]. The best bounds for μ and values for γ are listed in table 3.1 for dimensions one through five. The critical exponent γ is altered for a grafted chain that is anchored from one end to a wall, hence residing in a half-space. Additionally, the value for the swelling exponent ν is presented in different dimensions. Connective constants[4] and exact enumerations[5] for SAW can be found in electronic form.

3.4.1 Translocation between two equilibria

The key idea presented by Sung and Park [80], and Muthukumar [57] is to assume two separate equilibria that each contain a grafted polymer chain, i.e. a polymer attached to a wall from one end. These chains have lengths of s and $N - s$, where s is the reaction coordinate and N is the total length of these two parts, see Fig. 3.1. The system entropy,

[4] http://mathworld.wolfram.com/Self-AvoidingWalkConnectiveConstant.html
[5] http://www.ms.unimelb.edu.au/∼iwan/saw/SAW_ser.html

d	μ	γ	γ'	ν
2	$[2.62002, 2.679192495]$	$\frac{43}{32}$	$\frac{61}{64}$	$\frac{3}{4}$
3	$[4.572140, 4.7476]$	1.162	0.69	0.588
4	$[6.742945, 6.8179]$	1		$\frac{1}{2} + corr$
5	$[8.828529, 8.8602]$	1		$\frac{1}{2}$

Table 3.1: In self-avoiding random walk, values for the connective constant μ and the surface critical exponent γ in dimension d [9, 24, 60]. Values for a grafted chain in half-space, denoted here as γ', are also given. For $d \geq 4$, $\gamma = 1$. Logarithmic corrections denoted by *corr* are made to the swelling exponent ν in $d = 4$. Refs. [13, 17, 45, 51]

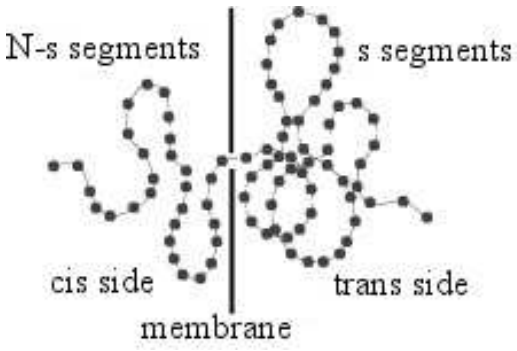

Figure 3.1: A schematic representation of the equilibrium polymer translocation. The chain length is $N - s$ segments on the cis side and s segments on the trans side.

$S = k_B \ln Z$, where the partition function Z is obtained using Eq. (3.11):

$$Z(s, N) = Z(s)Z(N - s) \tag{3.12}$$

$$= \mu^N \left[s(N - s)\right]^{\gamma - 1}. \tag{3.13}$$

The (Helmholtz) free energy $F = U - TS$ can now be written as

$$\frac{F_s}{k_B T} = N \ln \mu + (1 - \gamma) \ln s(N - s) + \frac{s\Delta\mu}{k_B T}, \tag{3.14}$$

where $\Delta\mu$ is the excess chemical potential per segment of the *trans* side relative to that of the *cis* side. The f_e derived from the free energy of Eq. (3.14) is written as

$$\frac{f_e}{k_BT} = -\frac{\partial}{\partial s}\frac{F_s}{k_BT} \tag{3.15}$$

$$= (\gamma - 1)\left[\frac{1}{s} - \frac{1}{N-s}\right] - \frac{\Delta\mu}{k_BT}. \tag{3.16}$$

The force f_e then contains two competing terms, the first, entropic term related to k_BT and the second, deterministic term related to $\Delta\mu$. The external driving force f that we use as a control parameter in our simulations is connected to the chemical potential difference as $f \sim \Delta\mu$. For unforced translocation, the control parameter $f = 0$.

The close-to-equilibrium criterion requires that the ratio of the translocation time and the (equilibrium) relaxation time of the polymer is small, $\tau/\tau_r \ll 1$. We shall discuss this ratio of times, as well as the relation of the entropic and deterministic terms, when we investigate the translocation process with simulations in Chapter 5.

3.4.2 Kramer's escape

When it was discovered that the previously presented equilibrium framework yielded unphysical results from the scaling of the translocation time with respect to the polymer length [15], the door was again open for other theories. Rate calculations and specifically the Kramer's escape problem was one potential candidate for solving the problem. Hence, we will briefly outline this specific problem before we try to apply it. For comprehensive literature about Kramer's work and rate calculations, see e.g. [32] and references there-in.

Consider independent Brownian particles in a potential $U(x)$, which has a shape shown in Fig. 3.2. Let us assume that the potential well is deep and that initially the particles are in the well. Physically, the particles are expected to reach a close-to-equilibrium state, but leak out slowly across the barrier. What is the rate at which this escape takes place? This is the Kramer's escape rate problem.

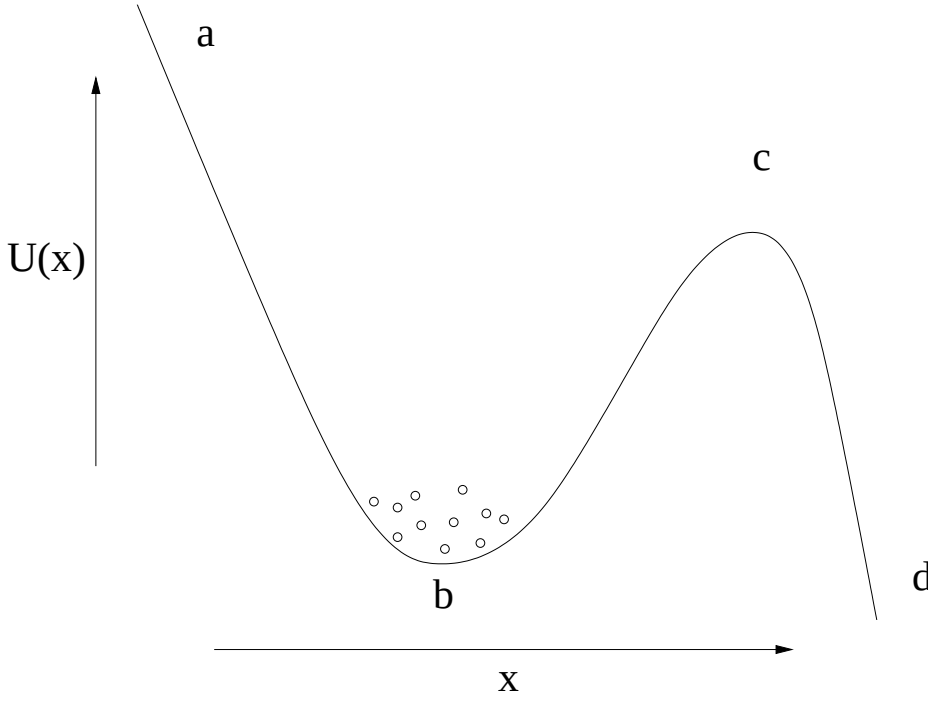

Figure 3.2: The generic shape of the potential $U(x)$ used in Kramer's problem as a function of the location x. An infinite potential wall **a** keeps the particles from escaping towards left. A well **b** is formed between the wall and a potential barrier **c**. The ensemble of particles in the well is close to equilibrium, as the particles slowly leak over the barrier into a state with lower potential **d**. The ingenuity in the formulation of Kramer's problem is that we do not have to know the exact shape of the potential $U(x)$. It suffices that $U(x)$ has this kind of a shape.

The Langevin equation for the particles in the overdamped limit, in which the inertial term $m\dot{v}$ is omitted, is written as

$$\xi v = -\frac{\partial U(x)}{\partial x} + f_r(t), \tag{3.17}$$

where $f_r(t)$ is the random force. The corresponding Fokker-Planck equation for the probability density $P(x,t)$ is given by

$$\frac{\partial P(x,t)}{\partial t} = \frac{\partial}{\partial x}\left[\frac{1}{\xi}\frac{\partial U}{\partial x}P(x,t)\right] + D\frac{\partial^2 P(x,t)}{\partial x^2} \tag{3.18}$$

$$= \frac{\partial}{\partial x}\left[\frac{1}{\xi}\frac{\partial U}{\partial x}P(x,t) + D\frac{\partial P(x,t)}{\partial x}\right] \tag{3.19}$$

$$= -\frac{\partial J}{\partial x}, \tag{3.20}$$

where $D\xi = k_BT$ and J is a probability density current

$$J = -\frac{1}{\xi}\frac{\partial U}{\partial x}P(x,t) - D\frac{\partial P(x,t)}{\partial x}. \tag{3.21}$$

After some algebra and a couple of saddle-point approximations [32], we essentially obtain the *Kramer's escape rate formula*

$$R_{kr} = \frac{D}{2\pi k_BT}\left[U''(b)|U''(c)|\right]^{\frac{1}{2}} \exp\left[-\frac{E_c}{k_BT}\right], \tag{3.22}$$

where $E_c = U(c) - U(b)$ is the barrier height. If the barrier height is raised, the escape rate falls off exponentially. The usefulness (or generality) of Eq. (3.22) comes from the fact that we only have to know the value of $U(x)$ at two points, $x = b$ and $x = c$. However, the formula only applies in the $E_c \gg k_BT$ regime, because of the assumptions we have made.

The application of Kramer's problem to the problem of polymer translocation can be attempted in two ways. The abstract entity of an 'escaping particle' can either be a single monomer or the polymer as whole. In the first case, the potential $U = U(\{x_j\})$ experienced by particle i is dependent not only on its own location but on the location of all the other particles as well. Hence, the assumption that the particles are independent cannot be satisfied. In the second case, the entropic potential of the polymer has a hilltop shape, which is completely different from what is required for Kramer's problem, see Fig. 3.2. The entropic potential $U(x)$ thus lacks the infinite wall that would confine the polymer into an entropic well. This deficiency can be compensated in two ways.

The infinite wall potential can be added to $U(x)$ by either restricting the first bead from being sucked into the pore [22, 21], or restricting the system space of the *cis* side. Polymer translocation from confinement has been studied in both planar [62] and spherical geometries. The latter is relevant especially in biological processes, e.g. bacteria inserting their DNA into living cells, which is often referred to as capsid ejection [40, 2]. However, these additions alter the system so fundamentally that the original problem what we wish to study becomes unaccessible. Moreover, in the limit of strong confinement the poly-

mer translocation is confinement driven [12], and thus in conflict with the equilibrium assumptions used in Kramer's problem.

3.5 Steady-state

The equilibrium framework offers an abundance of powerful tools [65]. Perturbation methods can expand some of these to cover non-equilibrium systems. One such method that uses the close-to-equilibrium assumption was the previously introduced Kramer's escape problem. In some cases, the statistical mechanical treatment can be extended to steady assemblies even if they are far from equilibrium [81]. The concept of equilibrium is then replaced by a so-called *steady-state*, and the statistical definitions of macroscopic quantities like temperature and chemical potential reduce to suitable averages over the local assembly. In other words, a system in a steady state has (numerous) properties whose averages are not changing in time. Systems with similar macroscopical properties, e.g. temperature, are *compatible* and can be brought together without any change in those properties [81]. However, there are restrictions to *compatibility* for systems that contain many-particle interactions.

If we consider our bead-chain polymer model, monomers cannot be taken as non-interacting particles. Hence, the sedimenting single polymer chains, studied in Article V, are not *compatible* to be brought together in the sense that the macroscopic properties of the steady-state would be conserved. In other words, single polymer chains in the dilute limit, where chain-chain interactions are negligible, are prone to have fundamentally different dynamical behavior than a system with more than one sedimenting chain would have.

In the polymer sedimentation problem of Article V the polymer resumes a settling velocity when the gravitational force is balanced by the viscous forces of the fluid. When the polymer has reached this settling velocity, we say it is in a steady-state for the purpose

of measuring some local quantities, e.g. the temperature and the radius of gyration R_G. For these, it is possible to determine a time-average, and thus combine data from different simulations to obtain the average. Hence, we assume that since the polymer actively tumbles through different configurations, it does not get stuck in any distinct area of the phase-space.

The average of the radius of gyration, that is constant in time, will turn out to be coupled with the hydrodynamical drag, with the time-dependent conformations resulting in fluctuations in the settling velocity. These velocity fluctuations can be considered through a concept of local temperature, as they show as a measurable *effective* diffusion for the center of mass. We shall return to this problem in Chapter 5.

4 Fluid dynamics

The study of the deformation and flow of matter – rheology – largely determines the dynamics of many biological structures. Hence, the implementation of hydrodynamics in a computational method is of high importance. However, this is not straightforward as any computational study is a compromise between two needs. First, the description of the structure and dynamics of the studied object should be detailed enough to allow for the observation of essential mechanisms, and second, the studied system sizes should be large enough to reach the experimentally relevant scales. There is no unique way to make this compromise, and therefore multiple methods with different pros and cons are generally employed.

In the preceding chapter, we discussed the Brownian heat bath, where hydrodynamics was completely ignored. However, it is common knowledge that hydrodynamics contributes even to equilibrium dynamics by adding long–range correlations between the suspended particles. This shows in, for example, polymer relaxation times [20]. If a sufficiently large external force is applied to a system, the system is no longer in equilibrium, and the Brownian motion becomes less important as the external force increases. In the limit where the thermal Brownian motion is negligible, hydrodynamics dominates. In the following, we shall discuss how the above–mentioned compromise between the level of detail and computational efficiency is coupled to the inclusion of hydrodynamics from the microscopic level to the macroscopic continuum limit, where the fluid is no longer presented by particles but by a field.

Microscopically, hydrodynamics can be correctly implemented only in the microcanonical ensemble, which preserves momentum. Using molecular dynamics, e.g. the GROMACS [23], to preserve the detailed interactions easily makes larger systems computationally intractable, thus making it impossible to investigate phenomena that show only on larger length scales. By a so-called dissipative particle dynamics [30] hydrodynam-

ics can be implemented judiciously and the detailed description of molecular dynamics be preserved, but if the simulated system does not allow for some additional coarse-graining, also dissipative particle dynamics tends to be prohibitively slow. The by now traditional coarse-grained complex fluid simulation method is the lattice Boltzmann method [7]. Its hybrid form where molecular dynamics is used to simulate objects like polymers in the solvent has proven relatively versatile [55].

The hybrid methods solve simultaneously the equations of motion for the particles and take into account the fluid in some coarse-grained manner, employing two time scales to achieve computational efficiency. Two of the models used for this Thesis, a coarse-grained complex fluid simulation method called the Stochastic Rotation Dynamics (SRD) used in Articles I and III, and a Navier-Stokes solver using the so-called immersed boundary assumption used in Article V, are both of hybrid form. These models differ from each other, and also from lattice Boltzmann method. For example, the particles describing the solvent dynamics in SRD are not restricted to lattice sites, as they are in the lattice Boltzmann method. SRD will be discussed in detail in Section 4.5.

In the continuum limit, the microscopic degrees of freedom are summed up in a field that describes the collective motion of the fluid [44]. The fluid field can then be simulated with a Navier–Stokes solver. In Article V, we employ such a solver with immersed boundaries [43, 42], i.e. that the fluid is assumed to fill the whole simulation box including the particle locations. We shall refer to it as the IB method in the following where we briefly introduce the macroscopic treatment of hydrodynamics.

4.1 From conservation laws to hydrodynamics

Assuming that the mass cannot be created or destroyed, we obtain the balance equation for mass, i.e. the continuity equation [44]

$$\frac{\partial \rho}{\partial t} + \nabla \cdot (\rho \mathbf{u}) = 0, \tag{4.1}$$

which states, that the change rate of mass inside a volume is equal to the mass flux through the surface of that volume. For incompressible fluid the density ρ is constant and the above equation reduces to

$$\nabla \cdot \mathbf{u} = 0. \tag{4.2}$$

Let us consider an arbitrary fluid element in an incompressible Newtonian fluid, with a volume V and surface S. The stress tensor σ is defined as [44]

$$\sigma = -p\mathbf{1} + \eta\big(\nabla \mathbf{u} + (\nabla \mathbf{u})^T\big), \tag{4.3}$$

where **1** is a second rank unit tensor, and p is the pressure. The viscosity η, which is the ratio between stress and the deformation, is assumed constant for a Newtonian fluid. The balance equation for momentum, in the coordinates of the fluid element, can now be written as [44]

$$\rho \frac{D\mathbf{u}}{Dt} = \nabla \cdot \sigma + \rho\, \mathbf{f}, \tag{4.4}$$

where **f** is the external force field. As noted before, for systems that are driven by a strong external force the thermal Brownian motion is negligible. Switching back to laboratory coordinates and by combining Eq. (4.3) and (4.4) we get the Navier-Stokes equation for the incompressible Newtonian fluid [44]

$$\frac{\partial \mathbf{u}}{\partial t} + (\mathbf{u} \cdot \nabla)\mathbf{u} = -\frac{1}{\rho}\nabla p + \nu \nabla^2 \mathbf{u} + \mathbf{f}. \tag{4.5}$$

Here $\nu = \eta/\rho$ is the ratio between the viscosity and the density, known as the kinematic viscosity. As in any other physical problem, the boundary conditions are a vital part of fluid mechanics, since material interfaces have certain properties that cannot be ignored. The typical physical boundary condition that is used in fluid mechanics is the no-slip

condition. It is the analog of the constitutive relations (the stress tensor σ defined in Eq. (4.3) and heat flux $\mathbf{q} = -k\nabla T$, where k is the thermal conductivity) and only holds when at least one material is a Navier–Stokes fluid (i.e. it obeys the Navier–Stokes equation) [44, 18]. The no-slip condition states that the microscopic fluid element residing on the surface of the particle does not have any movement relative to the surface, i.e. it moves with the surface.

The no-slip condition is inherent to both the SRD and the IB methods. In the first, the slit walls pose a strict no-slip condition to the fluid particles. The solute particles, in the first and in the latter, are imposed to such interactions with the fluid that the no-slip condition can be seen fulfilled. In addition, thermal fluxes are out of the scope of this Thesis, as it is assumed for all our models that the temperature varies slowly (if at all) so that no thermal convection occurs.

4.2 Reynolds number

Problems that require computational approach typically deal with non-linearity. For hydrodynamics, the non-linearity of the Navier-Stokes Eq. (4.5) is described by the dimensionless Reynolds number

$$\mathrm{Re} = \frac{VL\rho}{\eta}, \tag{4.6}$$

where V and L denote the characteristic velocity and length scales in the system and η is the viscosity. The Reynolds number is an estimate of the ratio of the inertial $(\mathbf{u}\cdot\nabla\mathbf{u})$ and viscous $(\eta/\rho\nabla^2\mathbf{u})$ terms in Eq. (4.5) presented in laboratory coordinates. Eq. (4.4) that is in the coordinates of the fluid particle can be presented in a dimensionless form, as a function of Re. For this purpose, we may introduce dimensionless variables (denoted by tildes) as follows

$$\mathbf{u} = V\tilde{\mathbf{u}}, \quad t = \frac{L}{V}\tilde{t}, \quad \frac{\partial}{\partial x} = \frac{1}{L}\frac{\partial}{\partial \tilde{x}}, \quad p = \rho V^2\tilde{p}, \quad \mathbf{f} = \frac{V^2}{L}\tilde{\mathbf{f}}. \tag{4.7}$$

Here V and L are the above–mentioned characteristic velocity and length scales that the flow has. Substituting these into Eq. (4.4), and dropping the tildes, we obtain the dimensionless Navier-Stokes equation

$$\frac{D\mathbf{u}}{Dt} = -\nabla p + \mathbf{f} + \frac{1}{Re}\nabla^2\mathbf{u}, \tag{4.8}$$

where Re $= VL/\nu$ is the Reynolds number as presented in Eq. (4.6). It should be noted here that in the IB method used in Article V, the single particle Re$= 0.25$ that we keep fixed could, in fact, be used as a control parameter. For SRD, we have approximated in Article I that the single particle Re $= VL/\nu \simeq 0.005$ in forced translocation with $f_{tot} = 3$, $N = 100$, $V = 0.004$, and $L = 1$. The kinematic viscosity for the bead used here is four times the one of the fluid $\nu = 3.1$, which is derived in Section 4.6. The whole polymer's Reynolds number is naturally larger (and dependent on the chain length N), since the polymer has a different characteristic length scale than a single particle.

4.3 Stokes approximation

Neglecting the inertial term $(\mathbf{u} \cdot \nabla\mathbf{u})$ from Eq. (4.5), we end up with an approximation $\mathrm{Re} = 0$, which is the so-called Stokes approximation. This approximation linearizes the Navier-Stokes equation (Eq. 4.5) and allows further analytical treatment. The equation thus reduces (when inertial and temporal acceleration $\partial\mathbf{u}/\partial t$ terms are ignored) to the Stokes equation

$$-\eta\nabla^2\mathbf{u} = -\nabla p + \rho\mathbf{f}. \tag{4.9}$$

With this approximation the problem of a single, non-Brownian, spherical particle of radius a and mass density ρ_p settling steadily in a gravitational field of strength g through an (incompressible) viscous fluid of mass density $\rho = \rho_p - \Delta\rho$ and shear viscosity η can be solved. The viscous force $6\pi\eta a u$ acting on the particle is balanced by the gravitational force $mg = \Delta\rho a^3 g$. The sphere then assumes a steady settling velocity

$$u \equiv \frac{2}{9}a^2\Delta\rho g/\eta, \tag{4.10}$$

where the fluid velocity field

$$\mathbf{u}(\mathbf{r}) \sim \frac{1}{r},\ r > a \tag{4.11}$$

decays very slowly as a function of distance r from the center of the sphere. A finite Reynolds number increases the decay dramatically.

The polymer in the sedimentation problem of Article V may be thought to be approximately a settling particle, whose hydrodynamic radius is represented by the radius of gyration R_G that was introduced in Section 2.3. In the forced polymer translocation, Storm et al. [79] considered the polymer as a particle of a radius R_G that is pulled towards the pore so that the pulling pore force is balanced by the hydrodynamic drag of a particle with radius R_G. However, this qualitative picture turned out to be inadequate, and a more suitable description was later given by Sakaue [69] and tested by us in Article I.

4.4 Péclet number

The Péclet number Pe$= Va^2/D$ is a dimensionless quantity measuring the relative importance of flow and thermal diffusion in a suspension. Consider a Brownian sphere of radius a that has a buoyant weight (i.e. weight minus the weight of solvent displaced) Δmg, where g is the acceleration due to gravity and Δm is the buoyant mass, settling through a viscous fluid at temperature k_BT in energy units. The Péclet number for this particle is obtained as [64]

$$\mathrm{Pe} = \frac{\Delta mga}{k_BT}, \tag{4.12}$$

since the settling velocity $u = mg\zeta$ and $D = k_BT/\zeta$ from Einstein relation, where ζ is the coefficient of the viscous drag on the fluid. Eq. (4.12) is seen to be simply the effective gravitational potential energy difference across a height equal to the particle radius a, scaled by the temperature. A system in which Pe is exceedingly large, 10^2 or more, the Brownian motion can be neglected [64]. The density difference between the particles and fluid $\Delta\rho$ in the IB method used in Article V is 1.5 times the density of the

fluid, thus $\Delta\rho = \rho_p - \rho = 1.5\rho$. Let us consider a suspension in the room temperature ($T = 293K$), in which $\mathrm{Pe} = 100$, for example. This would mean that the sedimenting particles (assumed to be spheres) of Article V would have a radius of about $1.6\,\mu\mathrm{m}$ and a mass of $2.5 \times 10^{-14}\mathrm{kg}$.

4.5 Stochastic Rotation Dynamics

The Stochastic Rotation Dynamics (SRD) – also called Multi-Particle Collision Dynamics – method was introduced by Malevanets and Kapral [52, 53, 54]. It is essentially a simplification of molecular collision dynamics yielding the correct hydrodynamic equations over long distances. By construction, the dynamics conserves mass, momentum, and energy. The algorithm consists of two phases, namely free streaming of the fictitious fluid particles and simplified collisions among them. For a system of Q fluid particles the free streaming step reads as

$$\mathbf{r}_i(t + \Delta t) = \mathbf{r}_i(t) + \mathbf{v}_i(t)\Delta t, \tag{4.13}$$

where $\mathbf{r}_i(t)$ and $\mathbf{v}_i(t)$ are the position and the velocity of particle $i \in [1, Q]$, respectively, and Δt is the time step of the algorithm. The free streaming is followed by the simplified collision step

$$\mathbf{v}_i(t + \Delta t) = \underline{\mathbf{R}}[\mathbf{v}_i(t) - \mathbf{v}_{cm}(t)] + \mathbf{v}_{cm}(t), \tag{4.14}$$

where $\underline{\mathbf{R}}$ is the rotation matrix and $\mathbf{v}_{cm}$ is the center-of-mass velocity. At each time interval the rotation axis is picked randomly, so that the rotation angle $\alpha = 3\pi/4$ is kept constant. In order to maintain molecular chaos, several different rotations have to be performed at different positions in the system. The simulation space is divided into cells, which are shifted randomly in the periodic y-direction between the time steps. Shifting ensures Galilean invariance at low temperatures $kT \ll 1$ [35]. An individual $\underline{\mathbf{R}}$ is defined for each cell, and accordingly for each cell $\mathbf{v}_{cm}$ is then defined as the center-of-mass

velocity of particles belonging to that cell, i.e.

$$\mathbf{v}_{cm} = \frac{\sum_{i=1}^{Q'} m_i \mathbf{v}_i(t)}{\sum_{i=1}^{Q'} m_i}, \tag{4.15}$$

where Q' is the number of particles in the cell and m_i is the mass of particle i. Hence the collision step, Equation (4.14), for each cell can be viewed as first eliminating the collective motion of the particles in the cell $\mathbf{v}_i(t) - \mathbf{v}_{cm}(t)$, then rotating the resulting random velocities to mimic collisions, rescaling them so that the equipartition theorem condition

$$\sum_{i=1}^{Q'} \frac{1}{2} m_i \left[\mathbf{v}_i(t) - \mathbf{v}_{cm}(t)\right]^2 = Q' \frac{3}{2} kT \tag{4.16}$$

is met and finally adding back the collective motion. The computational efficiency is thus obtained by taking the fluid particles' collisions into account statistically as an average over an ensemble of fictitious fluid particles.

Due to the simple coarse-grained fluid dynamics, implementation of a hybrid SRD, where the dynamics of the object under investigation is performed in more detail, is straightforward. The particles belonging to the investigated solute structure, such as the beads of a polymer, perform both molecular dynamics and SRD dynamics, and are thus coupled to the solvent. Accordingly, each solute particle is treated exactly like a solvent particle inside a cell. Additional computational efficiency is gained if the modes of motion of the solute and the solvent particles are well separated, by demanding that the masses of the solvent and solute particles differ. In the model used for Articles I and III, the solvent polymer beads are four times heavier than the fictitious solvent particles, which in a situation where the system geometry does not tend to decouple polymer from the solvent allows us to perform one SRD step for only every 500 molecular dynamics steps. However, due to the nature of the polymer translocation problem, the SRD steps are performed more often, once for every 50 molecular dynamics steps. This choice for the time parameter will be shortly justified.

The basic geometry used in the simulations for Articles I and III is a simulation box of $L_x \times L_y \times L_z$, where $L_x = 25$ and $L_y = L_z = 32$ in cell lengths. Having a fluid density of

5 solvent particles per cell, this equals to having approximately 128000 solvent particles in 25600 cells, in total. The simulation space is bounded by two walls perpendicular to the x direction. No-slip boundary conditions are applied between the walls and the solvent by reversing the velocity vectors of colliding particles, and the system is periodic in the y and z directions. However, the space is divided in two equally large compartments by a wall on the xy-plane. The polymers immersed in the solvent have segment lengths around 1, so typically there are from 1 to 3 polymer beads in one cell.

4.6 Schmidt number

The importance of hydrodynamic transport compared to diffusion can be characterized by the Schmidt number, Sc. It is defined as the ratio of momentum diffusivity (viscosity) to mass diffusivity, i.e. $Sc = \nu/D$, where ν is the kinematic viscosity. Most importantly, the Schmidt number distinguishes the dynamical behavior of fluids $Sc \simeq 10^2 - 10^3$ from that of gases $Sc \simeq 1$ [11]. In order to make accurate simulations, it is a good idea to verify that a model solvent represents what it is supposed to, which in this case is water. The IB method used in Article V does not contain thermal diffusion, so the Schmidt number is large (or infinite) — describing a liquid. For SRD, the total viscosity $\eta = \rho\nu$ consists of two terms [38, 35]

$$\eta = \eta_{kin} + \eta_{col}, \tag{4.17}$$

where

$$\eta_{kin} = \frac{k_B T \rho \Delta t}{a^3}\Big(\frac{5\rho}{(4 - 2\cos\alpha - 2\cos 2\alpha)(\rho - 1)} - \frac{1}{2}\Big), \tag{4.18}$$

$$\eta_{col} = \frac{m(1 - \cos\alpha)}{18 a \Delta t}(\rho - 1) \tag{4.19}$$

are the kinetic and collisional contributions. The Schmidt number can be adjusted with the choice of the collision time step Δt [67]. For our choice of parameters used in Articles I and III ($m = 4, \alpha = 3\pi/4, \Delta t = 0.1, a = 1, \rho = 5, k_B T = 1$), we have $\eta_{kin} \simeq 0.33$,

and $\eta_{col} \simeq 15.2$. Hence, the total viscosity $\eta \simeq 15.5$, and the kinematic viscosity $\nu \simeq 3.1$ for the solvent.

To obtain the Schmidt number, we also need to measure the diffusion coefficient D from our simulations. We consider a best–case scenario for the diffusivity of the solvent, by measuring the diffusion coefficient of a single monomer particle with $m = 16$, instead the one of a solvent particle with $m = 4$. We obtain $D_i \simeq 0.05$ from the mean-squared displacement for each component i in three dimensions. From $D = \sum_i D_i \simeq 0.15$ we obtain $Sc \approx 20$, which could now be four times lower for the sole solvent, since the solute monomer particles are four times heavier than the solvent particles. Judging from this, the solvent in our simulations describes a dilute liquid. However, since $Sc \sim 1/(\Delta t)^2$ [67], the Schmidt number for this model may be increased to obtain a better accordance with water (containing salt). This is done by decreasing the time step Δt with the caveat that computational efficiency is sacrificed concurrently.

4.7 Finite–size effects

Models that employ hydrodynamics typically have periodic boundary conditions to allow the formation and development of hydrodynamic modes at the longest possible length scale, which is the system size. In these cases, where the modes cross the periodic boundaries, it is crucial to distinguish actual physical behavior from model specific artefacts. All models need to be tested against *finite–size effects*, since any phenomenon that appears simply because the simulation box is too small is unphysical. In other words, we need to make sure that the size of the simulation box is large enough so that the finite–size effects are avoided.

With hydrodynamics, the primary concern is that the modes might couple through the mirror images of the simulation box and be unphysically strong. In our SRD translocation model, the slit walls on which the no-slip boundary condition is imposed effectively hin-

der forming of any periodic modes in the y-direction, and block them in the x-direction. Moreover, the pore wall restricts the fluid from forming periodic hydrodynamic modes in the z-direction, as even the pore is inpermeable to the fluid. Therefore, even when the box has periodic boundaries, periodic hydrodynamic modes are not allowed in the direction of the pore force. Somewhat in accordance, from our results concerning Articles I and III, a stronger finite–size effect than the potentially unphysical coupling of hydrodynamic modes resulted from the physical confinement of the polymer chain. Roughly, the requirement for the simulation box size is that a sphere of radius R_G fits easily to the *cis* side of the pore wall.

For the IB-method used in Article V, the system box of the computational model was also tested against finite–size effects, since periodic boundaries were used in all three dimensions. Too small a box was seen to alter both the static properties, such as the radius of gyration R_G, and dynamic properties, such as the terminal settling velocity v_{lim} and effective diffusion coefficient D, of the steady–state. While in steady–state, the settling polymer induces a backflow in the fluid, see Fig. 4.1. This figure is a snapshot illustration of the xz-plane, where z is the direction of the gravity, and the colors represent values $c_{x,z}$ from a norm imposed to the velocity of the fluid. Namely,

$$c_{x,z} = \sum_{y} [\mathbf{u}(x, y, z)]^2, \tag{4.20}$$

where $\mathbf{u}(x, y, z)$ is the fluid velocity in the grid point $\{x, y, z\}$. In Fig. 4.1, colors from highest to lowest value of c are red, yellow, light blue, and dark blue. Finally, the simulation box was chosen so large in the gravitational direction that the terminal velocity v_{lim} would not couple to the backflow of the polymer's own image. In order not to endlessly add more and more energy to the system, the algorithm is constructed so that the average fluid velocity is substracted from the fluid velocity in each grid point [43].

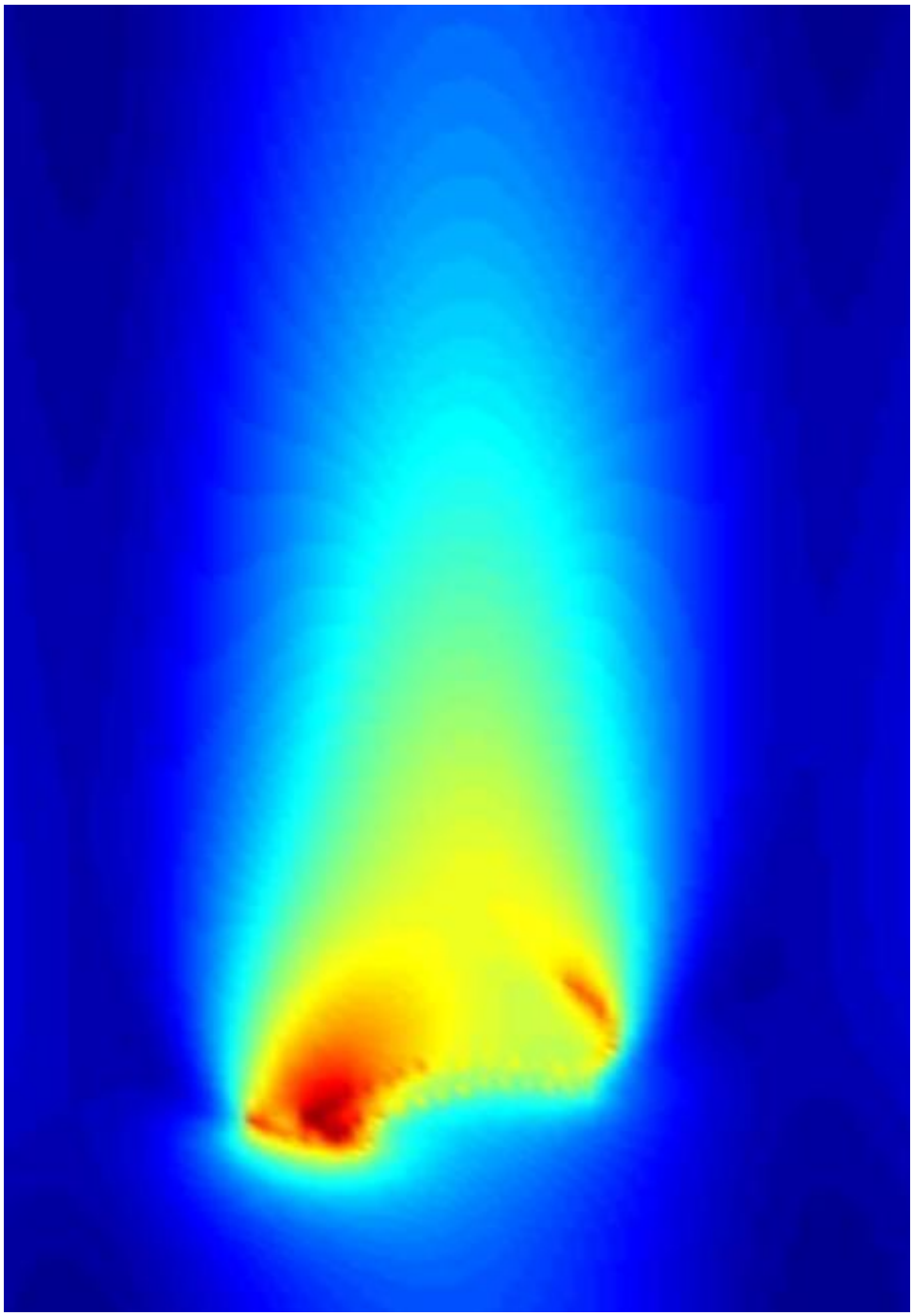

Figure 4.1: A snapshot of a system with a polymer of length $N = 64$ from the IB-method. The velocity field of the Navier-Stokes fluid is visualized by colors. The fluid is moving faster in the yellow and red spots than in the zone of blue color. This figure contains only information extracted from the fluid velocity field. We can identify some of the particle locations in the figure due to the immersed boundary condition, since the fluid and the particles travel at same velocity at these locations. The lighter blue arc following the polymer is the backflow. The figure does not display the whole simulation box.

5 Results

This Chapter contains the essential results presented in Articles I–V. The research in the polymer translocation reported in Articles I–IV is first reviewed by using the concepts introduced in Chapter 3. In particular, the equilibrium framework is invoked. Afterwards, the study of the sedimenting polymer in a steady–state far from equilibrium, reported in Article V, is outlined. Here, the emphasis is on the interplay between hydrodynamics and the polymer configuration.

5.1 Polymer translocation

The forced polymer translocation, which is relevant for e.g. ultra–fast DNA sequencing, has been said to be so well–studied experimentally that only the weak force regime was left for theoretical studies [41]. Close to equilibrium, when the driving force is weak, the transport mechanism is explained by the equilibrium framework (see Chapter 3). In translocation studies, however, the definition of a weak force is typically superficial. For example, requiring that $f_{tot}bN/kT \ll 1$ does not give quantitative information on how the simulation parameter f_{tot} should be set. Rigorously, the only way then is to test the equilibrium assumption. Otherwise, misinterpretations are possible. One example of this is to assume that equilibrium concepts apply also for strong forces, $f_{tot}b/kT = 1$ in Ref. [21].

In spite of the above statement in Ref. [41] several questions were, however, left open for theoretical studies. We will consider these in Section 5.1.2, after the critical evaluation of the equilibrium paradigm.

5.1.1 Critical evaluation of the equilibrium paradigm

At the time Article II was written, most of the computational research in polymer translocation was founded on the papers of Sung and Park [80] and Muthukumar [57], which use the equilibrium framework. Assumptions based on the equilibrium theory, *e.g.* the effect of the pore force and hydrodynamics, carried over to computational studies. Among other things, this hampered scientific dialogue as authors finding results inconsistent with the theory started arguing about the rigor of various results. Moreover, the research community was split in roughly two distinct camps. When others attempted to cement the universality of the forced translocation by pinning down the critical exponent(s), others tried to distinguish between the equilibrium and out-of-equilibrium processes and find separate solutions. Lately however, the community has become aware that instead of confirming the universalities expected by the equilibrium theory, the results cover different force ranges. For example, Sakaue [70] has defined three force regimes.

Monte Carlo (MC) methods have provided valuable results for polymers in equilibrium [20]. However, when a significant external force is present, the equilibrium assumption cannot be straightforwardly made. In Article II, we criticize the paradigm of using MC methods in forced translocation, i.e. the algorithms that have been proven strictly valid only for equilibrium dynamics. At the time Article II was written, the theoretical treatment of forced translocation can be said to have been almost solely guided by MC simulations, despite the MC results contradicting the available experimental results. Hence the theory evolved independently of the experimental findings. A lot of effort was wasted in the attempt to determine the dynamical universality class of the translocation process, by using the scaling of the average translocation time τ with respect to the polymer chain length N, $\tau \sim N^{\beta}$. As a result, there is an abundance of research reporting different scaling exponents β.

Already in 2005, Storm *et al.* [79] anticipated the experimental pore force magnitudes to be larger than those used in (MC) computer simulations. Unfortunately, they reported

experiments made with only one force value so that the assumption of a universal value for β was not proven wrong. In Article II (published in 2008), we showed that the experimentally and biologically relevant force range is beyond the force threshold for MC transition probability saturation. In other words, these forces cannot be simulated with MC methods. However, while close to equilibrium MC methods do yield the correct physical behavior and, at least in 1D, belong to the same universality class as LD simulations, which is also shown in Article II. We found it to be a somewhat general feature that the model specific details, e.g. hydrodynamics or the pore model, which might be insignificant close to equilibrium, were prone to become essential to out-of-equilibrium dynamics.

5.1.2 Research questions

In this Thesis, the main research questions concerning the problem of polymer translocation are $1.$ in what circumstances does the process remain close to equilibrium, and $2.$ how does the hydrodynamics contribute.

The first question is not to be taken lightly. It determines whether the dynamics of the process is predominantly deterministic or diffusive. We use the concept of equilibrium in a following manner. The fluctuation-dissipation theorem allows small perturbations when we consider the free energy. Then the mathematical tool derived from the assumptions is valid, and we consider the process to be close to equilibrium. In the forced translocation, we ask what is the threshold value for the pore force that just barely keeps the process in the frame that can be treated with equilibrium theory. The concept of equilibrium can thus be used to divide the problem of polymer translocation into (at least) two distinct cases. The first case is where the pore force is small enough so that it does not distort the probabilities of the system states. The second case is where the pore force dominates over any thermal based entropic forces. In the following, these are called as close-to-equilibrium and out-of-equilibrium cases, respectively. We shall reflect the concepts of

unforced (Article III) and forced translocation (Articles I-IV) upon this definition.

The second question is more concerned with the out-of-equilibrium process, since close to equilibrium the effect of hydrodynamics is less pronounced and better known, as discussed in Chapter 4. We are interested in the following questions: How is the dynamics affected, and is the hydrodynamic coupling through the pore essential? Close to equilibrium, the relaxation times of the polymer are affected. Hence, diffusion of the chain is faster. What then happens outside of equilibrium, when hydrodynamics mediate the momentum between the beads and thus enhance the collective motion of the polymer? Results from simulations including hydrodynamics are reported in Articles I and III.

5.1.3 Confirming the equilibrium statement

In order to confirm that the unforced translocation process takes place close to equilibrium, we investigate the state transition probabilities as is done in Article III. The polymer beads are numbered from 1 to N, with the middle bead initially in the pore and the end bead 1 on the *trans* and N on the *cis* side. The states of the system are labelled by the reaction coordinate s, defined as the number of the polymer bead currently in the middle of the pore. The system enters the state s, when the bead number s enters the middle of the pore. Assuming that the two polymer tails on each side of the wall are in separate thermal equilibria, we can calculate the transfer probability of a 'forward move' as $P_f(s) = P(s \to s+1) \sim \exp(-\beta(F_{s+1} - F_s))$, where $\beta = 1/k_B T$ and F_s is the free energy given by Eq. (3.14). We obtain

$$P_f(s) \sim \left(1 - \frac{1}{s} + \frac{1}{N-s}\right)^{1-\gamma}. \tag{5.1}$$

In our simulations, the pore is $3\,b$ long, so beads $s-1$ and $s+1$ are also inside the pore, which is taken into account by using effective values $s-1$ and $N-s-1$ for the chain lengths on *trans* and *cis* sides in Eq. (5.1).

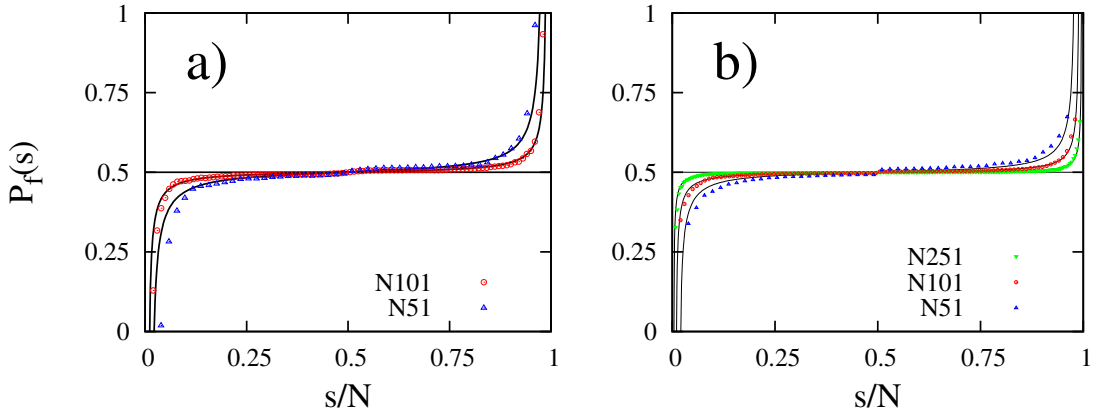

Figure 5.1: The forward move ($s \to s+1$) probability $P_f(s)$ for chains of length $N = 51$ and 101. The solid lines are theoretical predictions from Eq. (5.1), derived using the equilibrium free energy. The reduction of N due to finite pore length has been accounted for by using values of $N \in \{49, 99\}$ in theoretical predictions. a) SRD results where hydrodynamics is included and the pore is frictionless. The best fit (shown) is obtained with $\gamma = 0.69 \pm 0.05$. b) Results from Langevin dynamics in 2D with frictional pore, $N = 51, 101,$ and 251. The best fit (shown) is obtained with $\gamma = 0.80 \pm 0.05$.

In Fig. 5.1 a) the transfer probabilities obtained from the SRD simulations in 3D are compared to those given by Eq. (5.1). The best fit of the probabilities from both LD and SRD simulations to the analytical values is obtained for the exponent value $\gamma = 0.69 \pm 0.05$, which is the exponent for the self-avoiding walk (SAW) and hence in agreement with our measured value for the swelling exponent, $\nu = 0.60 \pm 0.02$, which for SAW is $\nu = 0.588$. Consequently, in 3D the unforced translocation is adequately described by two thermodynamic ensembles separately in thermal equilibrium, even in the presence of hydrodynamic modes. However, close to the chain ends, *i.e.* when s is close to 1 or N, translocating segments are inclined to accelerate due to the large entropic difference of the polymer segments on the two sides of the wall resulting in a large driving force. This has been studied in detail elsewhere [28].

The data in Figure 5.1 is somewhat rough, but further equilibrium behavior is observed in Article III considering the state transition times, and universality in scaling of the mean-squared displacement of the reaction coordinate s. Hence, we can conclude that

the unforced translocation process takes place close-to equilibrium.

Close to equilibrium, the critical properties, such as universality, are meaningful. In Article III, we verify the lower limit for the scaling exponent of the translocation time with respect to the chain contour length to be

$$\tau \sim N^{\beta} \, , \beta \geq 2\nu + 1, \tag{5.2}$$

which is a straightforward result from Rouse dynamics — i.e. without hydrodynamics — as proposed by Chuang *et al.* [15]. The idea behind Eq. (5.2) is that the polymer is considered to travel a distance proportional to its own characteristic length $R_G \sim N^{\nu}$ by diffusion. For the Rouse dynamics, $D \sim 1/N$ [20].

5.1.4 Force threshold

Let us (naively) assume that close-to-equilibrium and out-of-equilibrium regimes for the translocation process are separated by some force value, which we call the threshold pore force. In other words, if the total pore force surpasses this threshold value, the process is driven out of equilibrium. We can then use the forward transition probabilities $P_f(s)$ to determine an approximation for the threshold pore force value, as in Article IV. In Fig. 5.2, the measured $P_f(s)$ for various forces are shown. With $f_{tot} = 0.1$, the measured $P_f(s)$ is aligned with the solid line that represents the equilibrium transition probabilities, namely Eq. (5.1) shifted upwards. With $f_{tot} = 0.5$, the form of the measured $P_f(s)$ differs from the equilibrium form so that the process can be taken to be out of equilibrium. Therefore, $f_{tot}b/kT \simeq 0.1$ can be taken as the force threshold value for which the process is barely, but still, describable by the equilibrium framework.

Sakaue [70] theoretically distinguished three regimes, of which the close-to-equilibrium regime is one. The two other regimes are bound to reside out of equilibrium. We will try to separate these two, namely the high force range and the midrange, in Section 5.1.6.

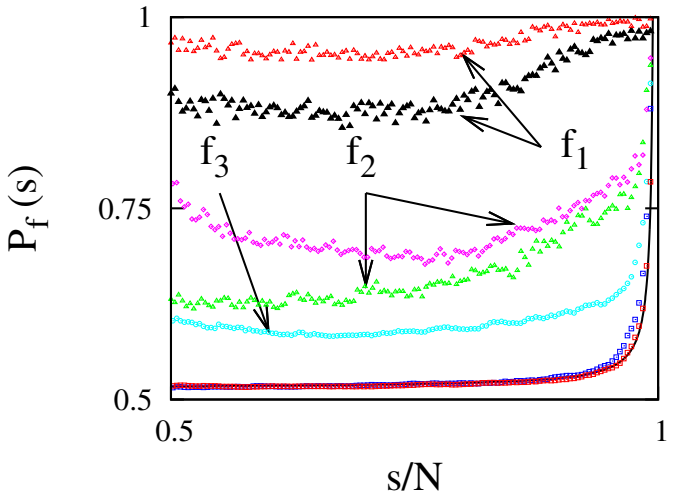

Figure 5.2: Forward transfer probabilities P_f as functions of the reaction coordinate normalized with polymer length, s/N. The data is from LD simulations and given for the bead (bd) and cylindrical (cyl) pore. Here $\xi = 0.7$ and N is 255 or 256, depending on the polymer's initial position. The pore force f_{tot} has the following values from top to bottom: $f_1 = 5.0$ (cyl,bd), $f_2 = 1.17$ (bd), $f_3 = 0.5$ (bd). At the bottom are P_f for $f_{tot} = 0.1$ for the bead (bd, distinct squares from the solid curve) and the cylindrical (cyl) pore (red) obtained from simulations together with the black solid curve calculated from Eq. (5.1) for the unforced case. For the f_{tot} values 0.1, 0.5, and 1.17 (f_2 upper curve) the polymer was initially placed halfway through the pore $s = (N-1)/2$. For the f_{tot} values 5.0 (both) and 1.17 (f_2 lower curve), the polymer started from the *cis* side $s = 1$. The shape of the probability curve depends of the pore model (f_1), polymer's initial position (f_2), and changes with the force.

5.1.5 The pore force in SI-units

Conventionally, as in our case, parameters and observables are presented in reduced, dimensionless units. How then do these units connect to SI-units, is what we attempt to address next. It is highly relevant to compare, for example, the simulation force magnitudes to the force magnitudes used in experiments and observed in biological processes.

The force mapping is considered in Articles I, II and IV. It is conveniently conducted by considering a dimensionless ratio of the two dynamically competing energies. We have used the ratio between the energy of the total force field, which is obtained from the

product of the pore force and the pore length, and the thermal energy, namely $f_{tot}b/k_BT$. This dimensionless quantity can be rather straightforwardly transformed from simulation units to SI-units by applying the according unit scales. We write the equality

$$\frac{f_{tot}b}{kT} = \frac{\tilde{f}_{tot}\tilde{b}}{k_B\tilde{T}}, \tag{5.3}$$

where the left and right hand sides consist of simulation and SI-units, respectively. Here, for example, $b = 1$ is the Kuhn length in simulation units, but $\tilde{b} = 2\lambda_p$ is in SI-units, where λ_p is the persistence length, roughly 40 Å for a single-stranded (ss) and 500 Å for a double-stranded (ds) DNA [82]. We note that the mapping of units is not unique, but depends on the physical system. Thus the simulated system can represent different systems found in nature that share some predefined characteristics. In our case, this means that DNA, RNA and proteins are all represented (at some level of abstraction) by our simulated polymer chain. Continuing with the mapping of units, the computational $kT = 1$ can be chosen to correspond to the product of the Boltzmann constant k_B, and the room temperature $\tilde{T} = 300K$. Hence, the dimensionless total pore force $f_{tot} = 3f$, where $f = 1$ corresponds to the force in SI-units $\tilde{f}$. From Eq. (5.3), we obtain $\tilde{f}_{tot} \approx 0.12$ pN for dsDNA and $\tilde{f}_{tot} \approx 1.6$ pN for ssDNA as in Article I. The threshold pore force value determined previously (as in Article IV) would then be 0.004 pN for dsDNA and 0.53 for ssDNA. This is what we obtain for the pore force by converting our simulation parameters from the simulation units to SI-units.

A typical experimentally used potential driving a polymer through the pore for both the ssDNA in the $\alpha-$hemolysin and dsDNA in the solid state pore is ~ 120 mV. The primary control parameter (in a regulating sense) is the total pore force, $\tilde{f}_{tot} = M\tilde{f}$, where M is the number of points on the polymer contour on which the pore force, $\tilde{f}$, is exerted. On dsDNA these points can be taken to reside at intervals determined by the nucleotide spacing, which is 3.4 Å for dsDNA and ≈ 4 Å for ssDNA. The pore force per nucleotide in the experiments may be estimated as

$$\tilde{f} = \frac{zq^*U}{L}, \tag{5.4}$$

where the pore potential $U = 120$mV, L is the length of the pore and the number of elementary charges e per nucleotide is $z = 2$ for dsDNA and $z = 1$ for ssDNA. The effective charge q^* is taken as e for dsDNA [79] and $0.1e$ for ssDNA due to charge reduction [73]. This gives $\tilde{f} \approx 1.92$pN for dsDNA and $\tilde{f} \approx 0.37$pN for ssDNA. Since the length L of the solid state pore is 20 nm, $M \approx 59$, $\tilde{f}_{tot} \approx 113$ pN or greater for dsDNA, but could also be considerably smaller due to Manning condensation and also due to the confinement in the pore. For ssDNA in an α-HL pore the charge reduction was evaluated to be drastic, giving $\tilde{f_{tot}} \sim 5$ pN [56, 73].

In spite of the intricacies (see Articles I, II and IV) involved in estimating the true force exerted on the polymer inside the pore, the experimental force magnitudes are included in the pore force range $f_{tot} \in [3, 300]$, used in the SRD simulations of Article I. The same qualitative out-of-equilibrium behavior that we observed was also verified with Langevin dynamics in Article II. In Articles III and IV, we have compared both the unforced and the close-to-equilibrium cases to the out-of-equilibrium case of forced translocation.

5.1.6 High pore forces

The limit where deterministic dynamics (originated by the external force) dominate over the stochastic one (originated by the thermal diffusion) can be found by considering the free energy. If the deterministic term is larger than the entropic term (that is bounded from above), we have

$$\Delta S < \frac{f_{tot} b}{kT}. \tag{5.5}$$

We can find out the maximum jump in entropy by requiring that the pore force is large enough to hold the first segment inside the pore, i.e. to hold the chain attached to the surface. We evaluate the entropy difference between a free and a grafted chain, as the

particle at the end of the chain can be either attached to the surface or not, to be

$$\Delta S = S_{free} - S_{grafted} \tag{5.6}$$

$$= (\gamma_f - \gamma_g) \ln N, \tag{5.7}$$

where $\gamma_f = 1.2$ and $\gamma_g = 0.69$ for three dimensions. The condition for $N = 100$, for example, now reads

$$\frac{f_{tot} b}{kT} \simeq 2.3 \, . \tag{5.8}$$

On the other hand, we may attempt to determine the magnitude of the total pore force for which the reaction coordinate s would increase with a probability $P_f(s)$ close to one, similarly as in Article IV. The random force term $f_r(t)$ in the Langevin equation of motion is approximated to be Gaussian with a standard deviation of σ (Ref. [65] pp. 251-253). The properties of the Gaussian standard deviation σ guarantee that if $f_{tot} \geq \sigma$, there is a probability of 0.68 that the total pore force is larger than the random force, and therefore the particle is bound to move in the wanted direction with a very high probability. Using the definition from fluctuation-dissipation theorem to obtain σ, we write the condition

$$f_{tot}^2 = \langle f_r(t) f_r(t') \rangle \tag{5.9}$$

$$= (\sigma)^2 \tag{5.10}$$

$$= 6 \, kT \xi \delta(t - t'). \tag{5.11}$$

For the simulation parameters $b = 1$, $\xi = 0.7$ and $kT = 1.2$, this condition yields

$$\frac{f_{tot} b}{kT} \simeq 2.2 \, . \tag{5.12}$$

In Articles I, II and IV, we note that the control parameter for the polymer translocation process is the total pore force, or equivantly in the case of an isotropic pore, the pore potential. In other words, the pore length is also a factor. In this sense, the calculated magnitudes of f_{tot} in Eqs. (5.8) and (5.12) are to be considered as total external forces experienced by the polymer. Finally, for $f_{tot} \simeq 4.2$ the process would be deterministic to the extent that $P_f(s)$ is close to unity, meaning that the thermal motion would be

negligible. For comparison, the process is shown to be clearly out of equilibrium for $f_{tot} = 3$, which is a value smaller than the respective biological or experimental force (in Article I), and also to reside out of equilibrium already for a considerably lower force $f_{tot} = 0.5$, see Article IV.

Translocation into a different dimension

An interesting special case of forced translocation is when the driving force originates from an entropic difference. This so–called pore escape is studied in Article III. Here we briefly show that the entropic force for a polymer moving from a space of smaller dimension into a space of larger dimension is large and that it effectively is a constant.

The equation (3.13) describes a polymer translocating between two equilibria of the same dimension $d_{TRANS} = d_{CIS}$. However, if one considers a case, where a polymer would exit a one–dimensional tubular hole, $d_{TRANS} > d_{CIS}$, the entropic force would be significantly larger than in Eq. (3.16). The partition function for such case is

$$Z(s, N) = Z^{3D}(s)Z^{1D}(N - s), \tag{5.13}$$

where $Z^{3D}(s)$ comes from Eq. (3.11), and $Z^{1D}(N - s) = 1 =$ constant, yielding

$$Z(s, N) \simeq \mu^s s^{\gamma-1}. \tag{5.14}$$

The free energy, $F_s/kT = -s \ln \mu + (1 - \gamma) \ln s$, yields a force

$$f_e = \ln \mu + (\gamma - 1)\frac{1}{s}, \tag{5.15}$$

for which $\ln \mu \gg |(\gamma - 1)/s|$, since $\ln \mu^{3D} \simeq 1.54$ and $\gamma - 1 \simeq -0.31$. Hence, the entropic force of Eq. (5.15) can be taken as a constant.

5.1.7 Ways of testing the equilibrium assumption

Although we have already shown using $P_f(s)$ that the translocation process is close to equilibrium when $f_{tot}b/kT \lessapprox 0.1$, and outside equilibrium when $f_{tot}b/kT \gtrapprox 0.5$, we shall discuss here some other ways to test the equilibrium assumption. This seems relevant, as there is no unique best way (in general) to determine whether a process is in or out of equilibrium. The following schemes were considered at some point during the making of this Thesis.

Basically, if given enough time, any isolated system reaches equilibrium. Therefore it is logical to check the (equilibrium) relaxation time τ_r of the polymer against the average translocation time τ. From this comparison we see if the polymer has enough time to relax so that the translocation process would take place close to equilibrium. For a rigorous comparison, we write

$$\begin{aligned} \lim_{t^* \to \infty} \int_0^{t^*} \exp\big(-\frac{t}{\tau_r}\big)\, dt \\ \equiv \tau_r, \end{aligned} \tag{5.16}$$

where τ_r is the characteristic equilibrium relaxation time, and t^* denotes time the polymer is let to relax. In the straightforward comparison of τ and τ_r, the problem usually is that t^* is finite. In other words, *how* the comparison between the time scales should be done quantitatively is not straightforward, due to the relaxation time being a characteristic time describing the decay of correlations, whereas the translocation time is an absolute time describing the transport of mass.

Regardless of this difficulty, we may attempt a straightforward time scale comparison. It is meaningful to consider the time scales at the single transition basis, since for each transition the entropy term in the free energy is changed. For a grafted polymer with $N = 70$, we obtain a characteristic relaxation time $\tau_r = 180 \pm 40$ with respect to the radius of gyration in 3D Langevin dynamics simulations for $m = 16$ (Article III). In the forced polymer translocation, we have an average time $t(s)$ for each transition $s \to s + 1$

for $m = 1$ (Article IV). For $f_{tot} = 1.5$, the forced translocation proceeds with $t(s) \simeq 10$ for $N = 128$. With $f_{tot} = 0.1$, we obtain values for $t(s)$ that reside between 100 and 150, excluding the transitions near the end of the polymer. Finally with $f_{tot} = 0.01$, the typical transition times $t(s)$ lie between 130 and 300. Noting the bead mass difference, the above relaxation time should be four times larger when compared to the above transition times, and based on these times, we can not judge whether the process is close–to–equilibrium or not, even if f_{tot} is one order of magnitude lower than what was needed to obtain the distribution of equilibrium transition probabilities $P_f(s)$. It is unlikely that this inaccuracy would disappear even for a lower force, since for $f_{tot} = 0.01$ we have obtained $\beta = 2.2 \pm 0.1$, which already corresponds to the unforced case $\beta = 2\nu + 1 = 2.2$ for our model, see Article IV.

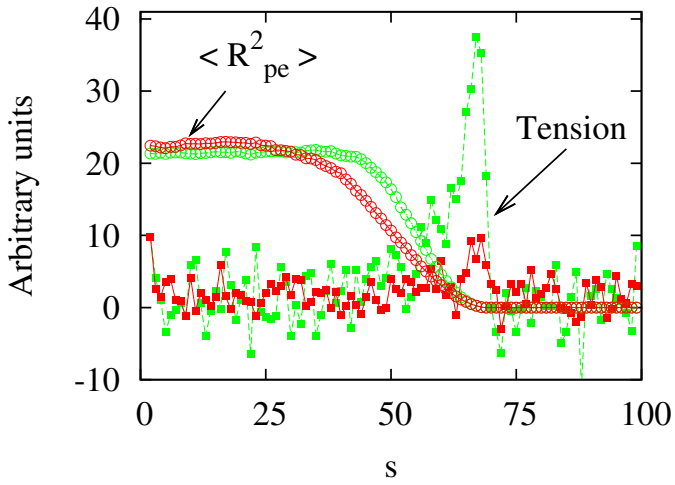

Figure 5.3: Comparison of two observables: the tension of labelled bond $k = 70$ and the mean squared pore-bead distance $\langle \delta R_{pe}^2 \rangle$ of the labelled bead $k = 70$ are both plotted as a function of s. The tension data is grainy, and although it has out-of-equilibrium characteristics for $f_{tot} = 30$, none can be seen for $f_{tot} = 3$. In contrast, $\langle \delta R_{pe}^2 \rangle$ has negligible fluctuations, and the observed plateau and decrease instead of a steady flat slope indicates that in addition to diffusion another kind of dynamics is involved. Obviously, $\langle \delta R_{pe}^2 \rangle$ is a more reliable and accurate observable for the system's behavior. The observables are extracted from the same data and thus contain an identical number of samples. These results are from 3D Langevin simulations with $N = 100$, and $f_{tot} = 3$ (red) and $f_{tot} = 30$ (green). A cylindrical pore with $d = 3$ was used.

One well-known way to find out if a system is out of equilibrium, is to measure tension. For the forced translocation, the tension of the bonds can be measured along the polymer contour. We measured the extension of the individual bonds, and determined the appropriate forces imposed by the FENE potential that are shown in Fig. 5.3. The tension turned out to be a bad measure for the non-equilibrium dynamics, since only for a total pore force $f_{tot} = 30$ we observe clear out–of–equilibrium characteristics.

A considerably better gauge for non-equilibrium dynamics was found by considering the monomer locations, more specifically the measured distances of the labelled polymer beads from the pore, R_{pe}. This can be seen from the comparison between the measured tension of a labelled bond and the measured mean squared pore-bead distance $\langle \delta R_{pe}^2 \rangle$ of a labelled bead, shown in Fig. 5.3. Observing the mean squared pore-bead distance $\langle \delta R_{pe}^2 \rangle$ as a function of the reaction coordinate s, we see that the behavior of the observable is drastically changed, when the tension imposed on the chain by the pore force reaches the labelled bead at the inflection points in Fig. 5.4 (a). From these points we extracted the the number of mobile beads s_m. We defined a labelled bead as mobile if the measured distance R_{pe}, averaged over several runs, changed appreciably. The extraction of s_m was possible only without hydrodynamics. For equilibrium translocation, one expects that $R_{pe}(s)$ would display only one dynamical region showing that the labelled bead is diffusing towards the pore.

In Fig. 5.4 b) s_m is plotted as a function of translocated beads s when hydrodynamics is not included. Linear dependence $s_m = ks$ is obtained. Up to lengths of $N \approx 200$, $k \sim N^{-\chi}$ and levels off to a constant value that is greater than unity for longer polymers. At all times, the total drag force, f_d, balances the total pore force f_{tot}. In the absence of hydrodynamics, all mobile beads experience an equal drag from the fluid viscosity. Hence,

$$f_d \sim s_m \langle v \rangle, \tag{5.17}$$

where $\langle v \rangle$ is the average velocity of the mobile beads. Without hydrodynamics, the beads are set in motion from their equilibrium positions, so the distance d of the mobile bead

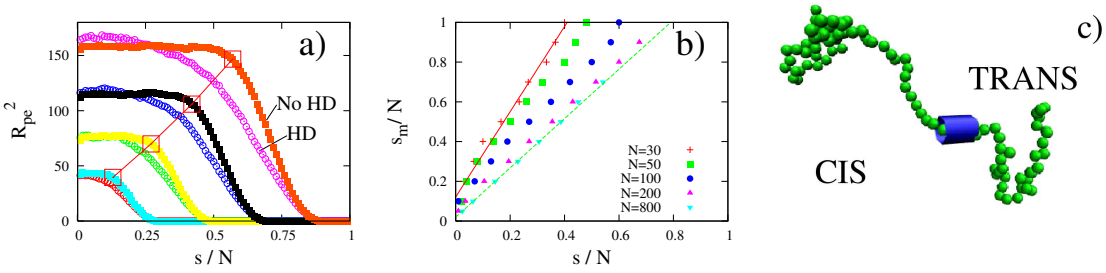

Figure 5.4: a) Averages over simulations of squared distances of beads numbered $30, 50, 70,$ and 90 from the pore as a function of the number of translocated beads s for polymers of length $N = 100$ with and without hydrodynamics. b) The number of mobile beads, s_m, (see text) vs number of translocated beads, s, both normalized to the polymer length, N, in the case of no hydrodynamics. $f_{tot} = 30$ in a) and b). c) 3D snapshot of a translocating polymer of length $N = 100$ at $s = 35$. Here the pore is frictionless and $f_{tot} = 6$. For clarity reasons, walls are not shown. The pore is frictional in a) and b).

furthest from the pore scales as $d \sim N^{\nu}$. The average translocation time then scales as $\tau \sim \langle d \rangle / \langle v \rangle \sim kN^{1+\nu} \sim N^{1+\nu-\chi}$. For the data in Fig. 5.4 b), where $f = 3$ ($f_{tot} = 9$), we obtain $\chi \approx 0.35$ that is in accord with the measured $\beta = 1.26$, see Fig. 1 b) in Article I. With the pore force $f = 100$ ($f_{tot} = 300$) the k's for $s_m = ks$ are smaller and the measured s_m-s curves for different N appear more aligned. Asymptotically, $k \to 1$, $\forall N$, as $f \to \infty$, *i.e.* polymer beads are translocated at the same rate that they are set in motion. Removing the friction from the pore also makes k values smaller and more identical for different N due to translocation becoming faster. Both the increase in the pore force and reduction in the pore friction take the scaling exponent β toward $1 + \nu$ due to s_m and hence the drag force, f_d, remaining more constant throughout the translocation. Hydrodynamics changes the form of the drag force. f_d no more depends strictly linearly on s_m for configurations of moving polymer segments, but all beads are set in motion in the beginning of translocation.

The R_{pe} consideration, residing entirely on the *cis* side of the pore wall, tells nothing about the dynamics on the *trans* side. To quantify the state of the *trans*-side chain, the radius of gyration R_G describes the compactness of the chain configuration. In Article I, the measured R_G was force-dependent, and statistically shorter than in equilibrium for

$f_{tot}b/kT \geq 3$, thus having a clear signature of out-of-equilibrium dynamics.

In summary, we discussed three ways to determine whether the process is out of equilibrium, in addition to the previously presented forward transition probabilities $P_f(s)$. Of these three, the pore to bead distance R_{pe} turned out to be a more sensitive observable than the transition times $t(s)$ or the chain tension. In addition, in Article IV we discuss that the model specific details, which were seen to be insignificant close to equilibrium but become increasingly dominating, when the process is driven out of equilibrium. In particular, we find that the scaling exponent β becomes dependent of the particle mass m, and that the pore model, whether a cylinder or constructed from beads, also alters β. Then the change in the scaling exponent β can also be regarded as an indicator of whether the process takes place close to equilibrium.

Additionally, hydrodynamics can also be thought to be a model specific detail. Next, we will review how it affects processes close and far from equilibrium.

5.1.8 Hydrodynamics significantly affects translocation taking place out of equilibrium

In our minimal model used in Article I (and III) fluid is not allowed to enter the pore, which precludes hydrodynamic coupling of the two chambers separated by the wall. As written in Article I and is implicitly evident from the following, we do not think that allowing hydrodynamics inside the pore would have an essential effect on dynamics. Here we discuss the forced translocation, where the pore force is the only driving force for the translocation.

The distribution of translocation times, $\pi(\tau)$, for polymers of length $N = 100$ is shown in Fig. 5.5. Due to the larger polymer velocities, i.e. the collective motion, the effect of hydrodynamics on forced translocation is much more pronounced than what was observed

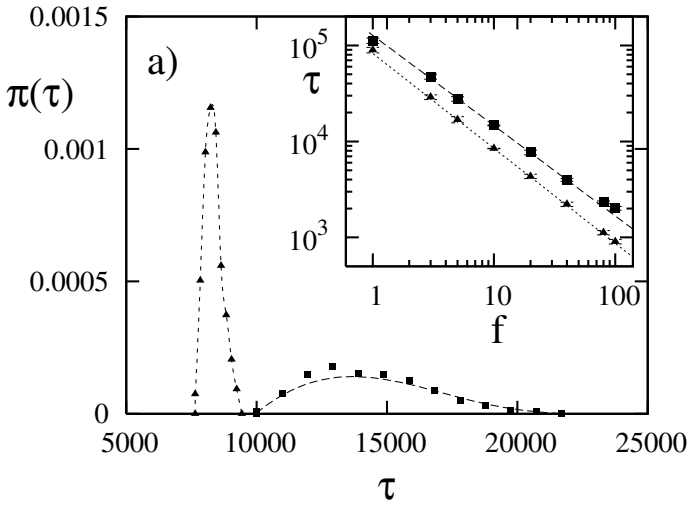

Figure 5.5: The distribution of translocation times τ for chains of length $N = 100$ and a constant pore force $f = 10$, with hydrodynamics (curve on left) (averaged over 300 runs) and without hydrodynamics (curve on right) (averaged over 400 runs). **Inset**: Average translocation time τ as a function of the driving force f. The scaling $\tau \sim f^{\alpha}$ is obtained with (higher plot) $\alpha = -0.940 \pm 0.013$ for $f \geq 3$, and (lower plot) $\alpha = -0.994 \pm 0.008$ for $f \geq 1$ without and with hydrodynamics, respectively. The chain length is $N = 100$, and the pore is frictional. The pore length $d = 3b$, so the control parameter $f_{tot} = 3f$.

for unforced translocation in Article III. In Article I, we observed a reduction in translocation times due to hydrodynamics, which was also seen by Fyta *et al* [26, 25]. In addition, hydrodynamics not only significantly speeds up forced translocation but also reduces the variance of measured translocation times. This is because the long range correlations due to hydrodynamics mediate the effect of the pore force along the polymer contour. The translocation times scale as $\tau \sim f^{\alpha}$, see in Fig. 5.5 (inset), which was expected for force values large compared with thermal fluctuations, $f_{tot}b/kT > 3$.

In Article I, the measured translocation times scale with polymer length, $\tau \sim N^{\beta}$, both with and without hydrodynamics. It is noteworthy, however, that there exists no single scaling, but β varies with the total pore force, $f_{tot} = 3f$. In our SRD simulations, β starts from unity and increases with f. For constant f, smaller β was obtained for the frictional pore. To distinguish between the change of β due to increasing translocation

velocity, v, and due to frictional term, when f was increased, scaling of τ with N for a pore with no friction was measured and it was found that the change of β was still significant, see Fig. 1 in Article I. The experimentally obtained $\beta \approx 1.27$ for a solid state pore [79] would be obtained in our model with a pore force $f \approx 3$ or greater. Hence, it can be concluded that the change of β with f arises not only from the change in the frictional contribution in the translocation dynamics, but also because of dynamic changes due to the change in v, which is a clear indication of out-of-equilibrium effects. In comparison, Fyta *et al.* [26] obtained $\beta = 1.28 \pm 0.01$, and $\beta = 1.36 \pm 0.03$ with and without hydrodynamics, respectively, for the pore force $f = 1$, which closely corresponds to $f = 1$ in our simulations as the pore length in [26] is approximately $3b$. A pore of very low friction was used in these lattice Boltzmann (LB) simulations. Accordingly, the obtained scaling exponent is in fair agreement with those we have obtained for the frictionless pore with hydrodynamics. Also the increase of β when hydrodynamics is switched off qualitatively agrees with our results.

When hydrodynamics is allowed, the polymer segments are moved from their initial equilibrium positions already before actually being pulled by the tightening polymer contour. This is seen in Fig. 5.4 a), where the squared distance, $R^2_{pe}(n)$, of the polymer bead, labelled n, measured from the pore on the *cis* side as a function of the number of translocated beads, s, is shown. In the absence of hydrodynamics, the segments towards the free end are seen to remain immobile until they are pulled towards the pore, whereas due to hydrodynamic interactions the distance of the labelled bead n from the pore is seen to start decreasing right from the beginning of the translocation. Hence, the initial configuration shows less in the translocation, when hydrodynamics is included. Instead, the segments on the *cis* side continually reach an increasingly extended polymer configuration. Regarding only the dynamics on the *cis* side, for an initially completely extended polymer asymptotically $\beta \to 1$ as f is increased, which explains the reduction of β at constant f when hydrodynamics is applied.

In summary, the inclusion of hydrodynamics essentially means adding large-scale many-

particle correlations, which emphasizes the collective modes in the dynamical behavior. Hydrodynamics is then naturally expected to have more impact on processes out of than those close-to-equilibrium where it mainly affects relaxation times and diffusive transport of the polymer. In particular, hydrodynamics mediates the pore force by emphasizing the collective motion of the beads, as we observed measuring R_{pe}^2 for $f_{tot} \geq 3$. As a result, average translocation times τ are decreased, and their distributions $\pi(\tau)$ are narrower. The force balance between the total pore force and the total viscous force experienced by the mobile beads governs the translocation dynamics. Because of this, the scaling exponent β is lower with than without hydrodynamics. Roughly, increasing the pore force in the polymer translocation problem shifts the interest from equilibrium theory into solving drift equations, e.g. Navier–Stokes. These are left for future studies.

Ignoring hydrodynamics is one reason for the previously–mentioned gap between computational and experimental results. In the light of the Monte Carlo, Langevin and SRD results, it can be said that running simulations is faster without hydrodynamics — with the caveat that the obtained results might not be comparable to experiments. We observed that hydrodynamics plays a significant role in the biologically and experimentally relevant force range of forced translocation (Article I).

5.2 Polymer sedimentation

In 1956, Zimm [86] introduced a theory which predicts that the sedimentation velocity of high molecular weight DNA will decrease as the rotor speed of an ultracentrifuge measurement increases. This inverse relationship leads to the fact that a lower molecular weight DNA may sediment faster than a high molecular weight DNA at high rotor speeds. The prediction of a crossover in sedimentation velocity, as the rotor speed is raised (to the order of 10^5 rounds per minute), has been experimentally verified [68, 14]. The crossover property is rather universal even when boundaries are applied. When a centrifuge tube is used, sedimenting particles interact with tube walls leading to a reduction in sedimentation velocity independent of the reduction described by Zimm's theory [16].

5.2.1 Research questions

When considering a polymer chain, one has a many-body object with complicated elastic and finite volume interactions — in addition to hydrodynamics — that guarantee a rich physical behavior at different length and time scales. The research questions concerning the polymer sedimentation are (i) what part of dynamics do we essentially lose, when thermal fluctuations are ignored, (ii) what is the relationship between the conformation of the sedimenting polymer and its limiting velocity, and (iii) what is the crossover limit in terms of N (for our model), when the sedimentation velocity starts to decline.

The first question concerns the applicability of the results in this study; what is the size and weight (in SI-units) of the particles that we study. In other words, we ask if our model depicts physical systems that can be found outside our simulations. Thermal motion, or a heat bath, adds perturbative forces that deviate the system from its possible ground state (given that one exists). If a system would get stuck in a ground state without any thermal motion, and could be excited out of that state with some, neglecting thermal motion would alter the dynamical behavior. We then ask if the sedimenting polymer is prone to get stuck

in some kind of a ground state while sedimenting. Moreover, we attempt to discover if the steady state (that the sedimenting polymer reaches) then resembles a ground-state from which the thermal motion could drive it out.

The second question is rather profound and in Article V we use a scaling theory to attack it. The external force, i.e. gravity, induces a limiting velocity and breaks the symmetry of the polymer conformation. Thus the separation between these asymmetric components depends only on the limiting velocity of the polymer.

The third question is motivated by the previously published theory and experiments. It is not concerned with new physics, as we try to reproduce something already discovered in experiments, but rather can act as a benchmark to our model.

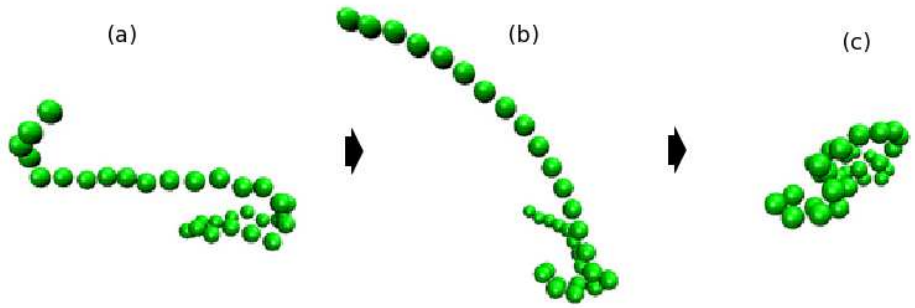

Figure 5.6: Snapshots of typical configurations of a settling polymer with $N = 32$ in the steady state. The polymer is elongated in the horizontal direction (a). The loose end of the polymer is attracted by the smaller pressure caused by back-flow, and the polymer elongates in the vertical direction (b). The spring forces pull the part that is left behind, and the polymer collapses into a globular shape (c), which then expands due to self-avoidance leading back to a shape of the type in (a).

5.2.2 Dynamics in a steady–state

The sedimenting polymer reaches a steady–state, when the gravity is matched by the hydrodynamic viscous force. The limiting settling velocity $v_{lim} \equiv \langle \mathbf{v}(t) \rangle$ of the polymer

is adequately described by the Stokes velocity of a sphere u_0 of Eq. (4.10). However, $v(t)$ has a time dependence that results from the altering conformations of the polymer, see Figure 5.6. This affects its effective radius and ultimately the viscous drag acting on the settling polymer. Hence, the component of the radius of gyration perpendicular to the gravitational force vector $R_{G,\perp}$ fluctuates, as shown in Figure 5.7. The time-series data (not shown) indicates a perfect correlation between the polymer's center of mass velocity and $R_{G,\perp}$. The tumbling of the polymer can be described as rather chaotic (temporal Fourier analysis showed no peaks corresponding to periodic oscillations).

Due to the time-dependence of $v(t)$ it is reasonable to treat it in a form where some small fluctuations $\delta\mathbf{v}(t) \ll v_{lim}$ are allowed keeping the main part v_{lim} constant,

$$v(t) = v_{lim} + \delta\mathbf{v}(t). \tag{5.18}$$

This approximation is particularly convenient, as it linearizes the Navier-Stokes equation for analytical purposes $v(t) \cdot \nabla v(t) \simeq v_{lim}\nabla\delta\mathbf{v}$. We will return to this later on. Some analytical results have been derived in [63].

Velocity fluctuations

In Chapter 3, we introduced means in form of Eq. (3.6) to determine the diffusion coefficient for a single particle. Similarly from the velocity fluctuations defined by Eq. (5.18), we determine an effective diffusion constant D_{eff} for the center of mass of the polymer. In the presence of the symmetry breaking gravitational field, we observed distinct scaling behaviors parallel to, and perpendicular to the gravitational field

$$\begin{aligned} D_{\parallel} &\sim N^{-\nu_{D,\parallel}}, \\ D_{\perp} &\sim N^{-\nu_{D,\perp}}. \end{aligned} \tag{5.19}$$

For both exponents, a negative value was obtained $\nu_{D,\parallel} = -1.0 \pm 0.2$ and $\nu_{D,\perp} = -0.22 \pm 0.11$. Hence, the effective diffusion coefficient D is increased when N grows.

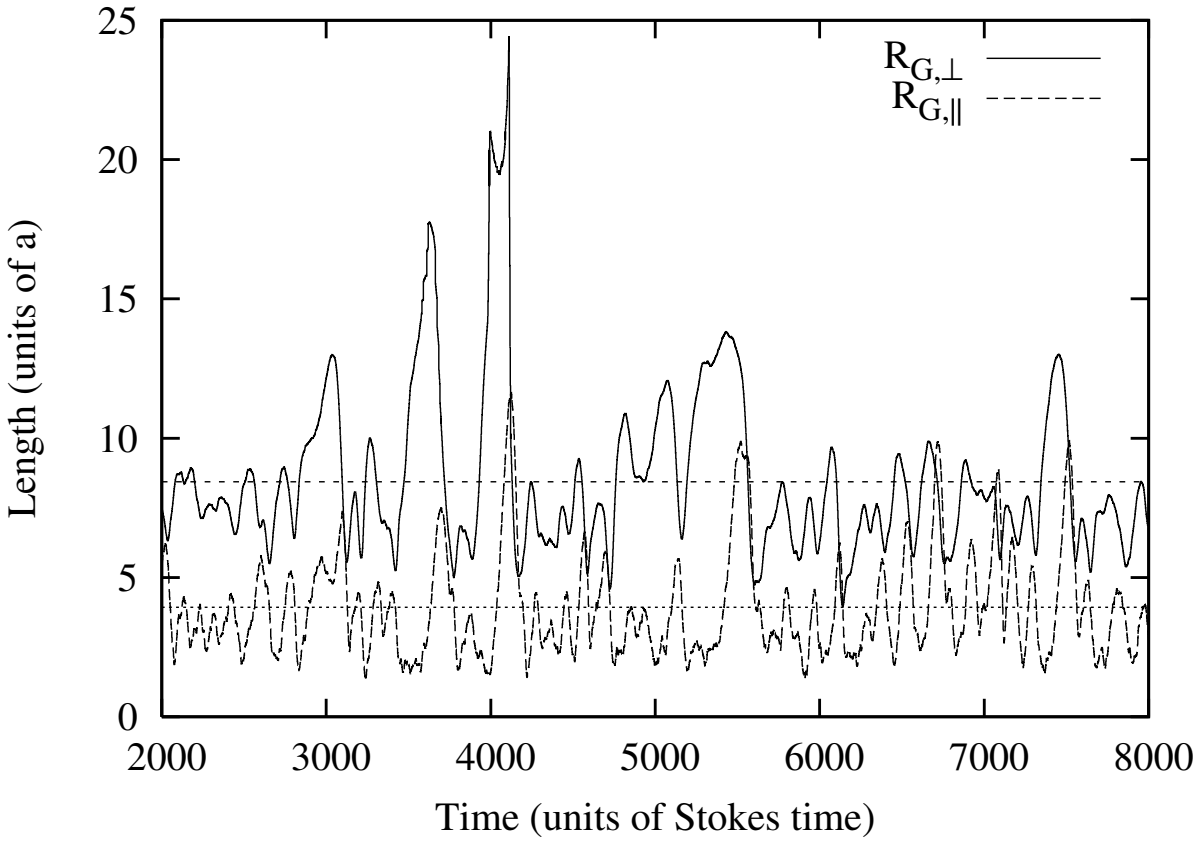

Figure 5.7: Raw data for the components of the radius of gyration with $N = 32$ in the steady-state. The vertical lines indicate the average value of the respective component, calculated from the whole simulation data, of which only a small part is shown in the figure.

This is in line with the fact that the total gravitational force acting on the polymer increases linearly as N grows, while the number of possible configurations through which the polymer 'chaotically' tumbles also increases. A broader insight on the scaling presented in Eq. (5.19) can be found in the dissertation of O. Punkkinen (pp. 90-91) [63].

To answer the first research question for the sedimentation problem, we wish to find out whether adding a heat bath to the simulations would reveal some new dynamical behavior. In the limit where thermal transport dominates, the diffusive dynamics of a polymer in equilibrium is well known [20]. In the limit where thermal transport is negligible, we

have the results of Article V. It is possible, but unlikely, that some additional underlying dynamics would be revealed as a result.

Essentially, the weight of the simulated particles is determined by the interactions that they experience. For very light particles, the gravitational force can be omitted, as Brownian forces dominate. For monomers that by themselves already experience the gravitational force, we can make a scaling estimate how the Peclet number for the polymer Pe$= VL/D$ depends on the chain length N. The flow is described by a characteristic velocity $V \simeq v_{lim} \sim N^{\beta-\nu_\perp}$ and a characteristic length $L \sim N^{\nu_\parallel}$. For details on the scaling of v_{lim}, see Article V. Using Zimm dynamics, the thermal transport for the center of mass declines $D \sim N^{-\nu}, \nu = 0.588$ as a function of N. We obtain

$$Pe \sim N^{\nu_\parallel+\beta-\nu_\perp+\nu} \simeq N^{0.93+\beta}, \tag{5.20}$$

where $\beta \geq 0.5$ is positive. This implies that the impact of the thermal transport decreases exponentially as a function of N, when the monomers are heavy enough to feel the gravitational pull. Comparing the effective diffusion of Eq. (5.19) to the thermal diffusion yields the same qualitative result: the first becomes more important with increasing N. Hence, the answer to the research question (i) is that adding the thermal motion is unlikely to reveal any interesting scaling dependencies with respect to N, as increasing N quickly takes the system to the limit of large Pe. Also, the chaotic conformational behavior that we have observed in Fig. 5.7 indicates that no such ground state exists, from which the polymer could be driven out by thermal fluctuations.

It is interesting to compare the chaotic shape fluctuations observed here to a study of polymer sedimentation in the limit Re $= 0$ [75]. In this case, for long polymers and large driving force (Pe large), chainlike polymers assume a stable, elongated configuration due to an effective stretching force on the chain. Our results indicate that such a configuration becomes unstable against hydrodynamic fluctuations for Re > 0, at least for large Pe. The particles that we have studied can be approximated as being in water at room temperature ($T = 293K$), where in the non-Brownian limit Pe $= 100$. Assuming a spherical shape,

we obtain a mass of 2.5×10^{-14} kg, and a radius of 1.6μm.

Conformations within the steady–state

In Article V, the steady–state of the polymer is determined by considering the average of R_G and the limiting velocity v_{lim} as time invariant for fixed N (as for an equilibrium system). To understand the conformational changes within the steady–state, we construct an equilibrium free energy function for the polymer as a function of $R_G(N)$, following the original Flory mean–field argument [20]. A kinetic term is added to take the non-equilibrium behavior into account [63]. Thus, the total energy of the polymer chain consists of the spring forces between the monomers, the self-avoidance and the kinetic energy contribution, and can be written as

$$E_{total} = \frac{1}{2}\frac{k}{N}R_G^2 + \frac{1}{2}\nu c^2 R_G^3 + \frac{1}{2}mN\left[\mathbf{v}(R_G)\right]^2, \tag{5.21}$$

where N is the number of monomers, k is the spring constant between two monomers, m is the mass of one monomer, and $c \simeq N/R_G^3$ is the concentration of monomers per volume. Furthermore, $\mathbf{v}(R_G)$ is the velocity of the center of mass for a given configuration R_G. As shown in Article V, the calculation then proceeds by using the approximation of Eq. (5.18) to treat the kinetic term. Essentially, omitting the steps already shown in Article V, we obtain

$$\begin{aligned} \langle R_{G,\perp} \rangle \sim & N^{2/3} |v_{lim}|^{1/3}, \\ \langle R_{G,\parallel} \rangle \sim & N^{7/12} |v_{lim}|^{-1/12}. \end{aligned} \tag{5.22}$$

In the case of the polymer chain, we can estimate the dependence of the limiting velocity on R_G by assuming that it is determined simply by the average size of the polymer in the direction perpendicular to gravity. Then, using the Stokes' formula introduced in Chapter 4, $6\pi\eta R|v_{lim}| = Mg$, where $M = Nm$ is the total mass of the polymer, we can derive that

$$v_{lim} \sim \frac{mN}{\langle R_{G,\perp} \rangle}. \tag{5.23}$$

In the limit of low Re, the scaling of the components of the radius of gyration is then given by $\langle R_{G,\perp} \rangle \sim N^{0.545}$ and $\langle R_{G,\parallel} \rangle \sim N^{0.818}$. These results are consistent with our previous assumption that $R_{G,\parallel} \gg R_{G,\perp}$ for large N.

At the limit of high Re, we use an empirical expansion formula for the limiting velocity, which is given by

$$\frac{Mg}{|v_{lim}|} = 6\pi R_{G,\perp}\eta\Big(1 + \frac{Re}{4(1+\sqrt{Re}} + 0.017Re\Big). \tag{5.24}$$

This is a theoretically convenient form, since at the limit $Re \ll 1$, Eq. (5.24) reduces to the Stokes equation. We can now write a general scaling form

$$v_{lim} \sim N^{\beta-\nu_\perp}, \tag{5.25}$$

where $\beta = 1$ for Re $\ll 1$ and $\beta = 1/2$ for Re $\gg 1$. Inserting this into Eq. (5.22), we obtain the theoretical results shown in Table I of Article V. The research question (ii) is answered by Eq. (5.25).

The qualitative behavior of the sedimentation velocity

To be in line with the experiments, the scaling behavior $v_{lim} \sim N^{1/2-\nu_\perp}$ should yield a negative exponent with Re $\gg 1$. Using the value $\nu_\perp = 0.45 \pm 0.07$ obtained from simulations, the settling velocity would scale as $v_{lim} \sim N^{0.05}$ for large N. The scaling exponent thus approaches, but never reaches, a negative value. Our study was limited to modest polymer lengths due to computational cost that increased as $\sim N^3$, and therefore it is likely that the negative exponent can only be observed for longer polymers.

In Article V, we have extrapolated from the R_G data that the $R_{G,\parallel}$ component would exceed the perpendicular component at $N \approx 120$. This might lead into dynamical changes incurring the crossover. Obviously, the range of N we studied was below the crossover value. The answer to the research question (iii) thus remains vague. As the crossover has

been experimentally observed and well known, the research question concerning only the benchmarking of the model is somewhat academic.

6 Conclusion

In this Thesis, two problems of polymer physics have been reviewed. First, the background for the problems of polymer translocation and polymer sedimentation was introduced in Chapter 1. Then the coarse–graining of molecular structures, necessary for construction of computational models, was outlined in Chapter 2. For the problem of polymer translocation we also introduced the widely used theoretical equilibrium framework in Chapter 3. In order to give a necessary background for hydrodynamics that is inherent to two of the five computational models used in this Thesis, an outline of the fluid dynamics was presented in Chapter 4. This concerned both the translocation and the sedimentation problem. Finally, the essential results of all of the Articles I–V have been presented in Chapter 5.

Here we present the summary of the results of this Thesis, and then discuss them.

6.1 Summary of results

In polymer translocation, we have asked first in what circumstances it is an equilibrium process, and second how the hydrodynamics contributes.

In Article II, we performed a critical evaluation of the equilibrium paradigm used in Monte Carlo studies. In particular, we showed that the experimentally and biologically relevant force range is above the force value for which the MC transition probabilities reach the value one. In other words, these forces cannot be simulated with MC methods. In contrast, close to equilibrium MC methods do yield the correct physical behavior and, at least in 1D, belong to the same universality class than LD simulations, which is shown in Article II.

In Article III, we confirmed that the unforced translocation process takes place in or close to equilibrium by investigating the (forward) transition probabilities $P_f(s)$ obtained from the equilibrium framework. Furthermore, we used the forward transition probabilities $P_f(s)$ to determine the threshold value for the pore force, for which the process is barely, but still, describable by the equilibrium framework (Article IV). In addition to this close-to-equilibrium regime, we estimated the total pore force values for the high force and middle regimes in Article IV, which were originally proposed by Sakaue [70].

We compared pore forces used in our simulations to those used in experiments by mapping the force through dimensionless energy units. In spite of the intricacies (see Articles I, II and IV) involved in estimating the true force exerted on the polymer inside the pore, the experimental force magnitudes were seen to be inside the pore force range used in the SRD simulations involving hydrodynamics (Article I).

We have discussed ways to test whether the system is close-to equilibrium, other than the direct measurement of the transition probabilities $P_f(s)$. These include comparing the (equilibrium) relaxation time to the transition times $t(s)$, measuring the tension along the polymer contour and, finally, tracing the distance of the labelled beads from the pore, which turned out to be a sensitive indicator of out-of-equilibrium behavior. There are other indicators, however. In Article IV, we have shown that the model specific details, which might be insignificant close to equilibrium can become increasingly meaningful or even dominating to the dynamics, when the process is driven out of equilibrium. In particular, we have found that the scaling exponent β becomes dependent of the particle mass m, and that the pore model, whether a cylinder or constructed from beads, also alters β.

Due to the larger polymer velocities, i.e. collective motion, the effect of hydrodynamics on the forced translocation (Article I) is much more pronounced than what we observed with the unforced translocation (Article III). Including hydrodynamics essentially means adding long–range many–particle correlations, which emphasizes the collective modes

in the dynamics. In Article I, we obtained a reduction in translocation times due to hydrodynamics, which was also seen by Fyta *et al* [26, 25]. In addition to significantly speeding up the forced translocation process, hydrodynamics also reduced the variance of measured translocation times. This is due to the induced long range correlations that mediate the effect of the pore force along the polymer contour. On the other hand, we feel that ignoring hydrodynamics is one reason for the gap between computational and experimental results. In the light of the Monte Carlo, Langevin and SRD results, it can be said that running simulations is faster without hydrodynamics. The caveat is that the obtained results might not be comparable to experiments, since we found that hydrodynamics plays a significant role in the biologically and experimentally relevant force range of forced translocation.

In the polymer sedimentation, we have asked (i) what part of dynamics do we essentially lose, when thermal fluctuations are neglected, (ii) what is the relationship between the conformation of the sedimenting polymer and its limiting velocity, and (iii) what is the crossover limit in terms of N (for our model), when the sedimentation velocity starts to decline.

In the limit where thermal transport dominates, the diffusive dynamics of a polymer in equilibrium is well known [20]. In the limit where thermal transport is negligible, we have the sedimentation results of Article V. It is unlikely that adding a heat bath in our simulations would reveal any new scaling behavior, since increasing the polymer length quickly takes the system to the limit of large Pe. Additionally, the polymer conformation exhibits such a chaotic time-development that no ground state from which the polymer could be driven out by thermal fluctuations is likely to exist.

A polymer sedimenting in the dilute limit assumes a steady–state. The polymer settles with a limiting velocity that is connected to the component of the radius of gyration perpendicular to the direction of the gravity. In Article V, we present a scaling law to quantify this connection. Additionally, an expansion to this scaling law is given with

respect to the Reynolds number. Hydrodynamic fluctuations for $\mathrm{Re} > 0$, at least for large Pe, cause the polymer to tumble, which chaotically alters its configuration.

Computational constraints prevented us to observe the theoretically and experimentally discovered crossover, where the increasing the chain length would decrease the settling velocity of the center of mass of the polymer.

6.2 Final remarks

In this Thesis, the discussion on the translocation problem has been twofold. First, we have discussed a problem of physics that requires a study revealing the underlying dynamics. This aspect is mostly covered by the summary of results, where the research questions were covered with their appropriate answers. Second, we have discussed the gap between the theoretical and experimental results in literature that originated from too general equilibrium assumptions in theoretical studies, while the experimental process was out of equilibrium. Perhaps the lesson to learn here is that one should be very careful with assumptions, especially since they are built into computational models.

Means like the equilibrium framework and excessively used MC simulations that can be credited for most of the static (equilibrium) results, e.g. critical exponents, have to be evaluated critically when applied on a new problem. The best paradigm that the writer is aware of is to use different models and compare the results. By doing so, the model specific details that might be first hidden are bound to be revealed.

Here, it all boiled down to distinguishing between out-of-equilibrium and close-to-equilibrium processes. As there currently is not any paradigm to do this separation, it had to be made using different indicators or measures. Although it felt sometimes like trying to draw lines on water, the separation based on the transition probabilities turned out to be quite successful in the end.

Philosophically, the coarse–graining paradigm in polymer physics often culminates in making scaling laws with respect to various parameters, e.g. the chain length. These laws express the inherent characteristic properties of the polymer systems studied in this Thesis, which we set out to explore in the Introduction. In other words, these scaling laws express an emergent level of physics arising from the basic equations of motion, which, reflecting to the paradigm, cannot be straightforwardly derived from these basic equations, nor be used as a constructionistic building part (or a piece of puzzle) to obtain the original system (the puzzle) that was studied.

In this Thesis, we have seen that equilibrium and out-of-equilibrium polymer systems may both have at least apparent characteristic scaling properties, even if the scaling behaviors differ and follow from different dynamics. It remains an open question, why we obtain apparent scaling behavior even for a process that we have shown to be nonuniversal. In spite of this, the coarse–graining paradigm proved valuable and took us through the above–mentioned problems in the sense that this work is finished.

References

[1] B. Alberts *et al*. 1994. Molecular Biology of the Cell. Garland Publishing, New York.

[2] I. Ali, D. Marenduzzo, and J. M. Yeomans. 2006. Polymer Packaging and Ejection in Viral Capsids: Shape Matters. Phys. Rev. Lett. 96, no. 20, page 208102.

[3] I. Ali and J. M. Yeomans. 2005. Polymer translocation: The effect of backflow. J. of Chem. Phys. 123, page 234903.

[4] M.P. Allen and D. J. Tildesley. 2006. Computer Simulation of Liquids. Oxford science publications, Oxford.

[5] P.W. Anderson. 1972. More is Different. Science 177, page 393.

[6] M. Bates, M. Burns, and A. Meller. 2003. Dynamics of DNA Molecules in a Membrane Channel Probed by Active Control Techniques. Biophys. J. 84, page 2366.

[7] R. Benzi, S. Succi, and M. Vergassola. 1992. The lattice Boltzmann equation: theory and applications. Physics Reports 222, no. 3, pages 145 – 197.

[8] M. Bernaschi, S. Melchionna, S. Succi, M. Fyta, and E. Kaxiras. 2008. Quantized Current Blockade and Hydrodynamic Correlations in Biopolymer Translocation through Nanopores: Evidence from Multiscale Simulations. Nano Letters 8, no. 4, pages 1115–1119. PMID: 18302329.

[9] W. A. Beyer and M. B. Wells. 1972. Lower Bound for the Connective Constant of a Self-Avoiding Walk on a Square Lattice. J. Combin. Th. A 13, pages 176–182.

[10] R. B. Bird, R. C. Armstrong, and O. Hassager. 1987/2001. Dynamics of Polymeric Liquids Vol. 1. Wiley-Interscience, New York.

[11] T. Bonometti and S. Balachandar. 2008. Effect of Schmidt number on the structure and propagation of density currents. Theor. Comput. Fluid Dyn. 22, page 341.

[12] Angelo Cacciuto and Erik Luijten. 2006. Confinement-Driven Translocation of a Flexible Polymer. Phys. Rev. Lett. 96, no. 23, page 238104.

[13] J.L. Cardy and S. Redner. 1984. Conformal invariance and self-avoiding walks in restricted geometries. Journal of Physics A: Mathematical and General 17, no. 17, page L933.

[14] David Chia and Verne N. Schumaker. 1974. A rotor speed dependent crossover in sedimentation velocities of DNA's of different sizes. Biochemical and Biophysical Research Communications 56, no. 1, pages 241 – 246.

[15] Jeffrey Chuang, Yacov Kantor, and Mehran Kardar. 2001. Anomalous dynamics of translocation. Phys. Rev. E 65, no. 1, page 011802.

[16] R. Clark and C. Lange. 1980. A quantitative test of Zimms model for the rotorspeed-department sedimentation of linear DNA-molecule. Biopolymers 19, pages 945–964.

[17] A. R. Conway and A. J. Guttmann. 1996. Square Lattice Self-Avoiding Walks and Corrections to Scaling. Phys. Rev. Lett. 77, no. 26, pages 5284–5287.

[18] Michael A. Day. 1990. The no-slip condition of fluid dynamics. Erkenntnis 33, pages 285–296. 10.1007/BF00717588.

[19] P. G. de Gennes. 1979. Scaling Concepts in Polymer Physics. Cornell University Press, Ithaca and London.

[20] M. Doi and S. F. Edwards. 1986. The Theory of Polymer Dynamics. Oxford science publications, Oxford.

[21] J. L. A. Dubbeldam, A. Milchev, V. G. Rostiashvili, and T. A. Vilgis. 2007. Driven polymer translocation through a nanopore: A manifestation of anomalous diffusion. EPL (Europhysics Letters) 79, no. 1, page 18002.

[22] J. L. A. Dubbeldam, A. Milchev, V. G. Rostiashvili, and T. A. Vilgis. 2007. Polymer translocation through a nanopore: A showcase of anomalous diffusion. Phys. Rev. E 76, no. 1, page 010801.

[23] Lindahl Erik, Hess Berk, and van der Spoel David. 2001. GROMACS 3.0: a package for molecular simulation and trajectory analysis. J Mol Model 7, page 306.

[24] S. R. Finch. 2003. Self-Avoiding Walk Constants. 5.10 in Mathematical Constants. Cambridge University Press, Cambridge, England, 331-339 pages.

[25] M. Fyta, E. Kaxiras, S. Melchionna, and S. Succi. 2008. Multiscale Simulation of Nanobiological Flows. Computing in Science Engineering 10, no. 4, pages 10 –19.

[26] M. Fyta, S. Melchionna, S. Succi, and E. Kaxiras. 2008. Hydrodynamic correlations in the translocation of a biopolymer through a nanopore: Theory and multiscale simulations. Phys. Rev. E 78, no. 3, page 036704.

[27] M. Gauthier and G. Slater. 2008. Molecular Dynamics simulation of a polymer chain translocating through a nanoscopic pore. The European Physical Journal E: Soft Matter and Biological Physics 25, pages 17–23. 10.1140/epje/i2007-10257-5.

[28] M. G. Gauthier and G. W. Slater. 2009. Nondriven polymer translocation through a nanopore: Computational evidence that the escape and relaxation processes are coupled. Phys. Rev. E 79, no. 2, page 021802.

[29] Kai Grass, Ute Böhme, Ulrich Scheler, Hervé Cottet, and Christian Holm. 2008. Importance of Hydrodynamic Shielding for the Dynamic Behavior of Short Polyelectrolyte Chains. Phys. Rev. Lett. 100, no. 9, page 096104.

[30] R.D. Groot and P.B. Warren. 1997. Dissipative particle dynamics: Bridging the gap between atomistic and mesoscopic simulation. J. Chem. Phys. 107, page 4423.

[31] S. Guillouzic and G. W. Slater. 2006. Polymer translocation in the presence of excluded volume and explicit hydrodynamic interactions. Physics Letters A 359, no. 4, pages 261 – 264.

[32] Peter Hänggi, Peter Talkner, and Michal Borkovec. 1990. Reaction-rate theory: fifty years after Kramers. Rev. Mod. Phys. 62, no. 2, pages 251–341.

[33] I. Huopaniemi, K. Luo, T. Ala-Nissila, and S.-C. Ying. 2006. Langevin dynamics simulations of polymer translocation through nanopores. J. of Chem. Phys. 125, page 124901.

[34] C. A. III Hutchison. 2007. DNA sequencing: bench to bedside and beyond. Nucleic Acids Res. 35, pages 6227–37.

[35] T. Ihle and D. M. Kroll. 2003. Stochastic rotation dynamics. I. Formalism, Galilean invariance, and Green-Kubo relations. Phys. Rev. E 67, no. 6, page 066705.

[36] Yacov Kantor and Mehran Kardar. 2004. Anomalous dynamics of forced translocation. Phys. Rev. E 69, no. 2, page 021806.

[37] John J. Kasianowicz, Eric Brandin, Daniel Branton, and David W. Deamer. 1996. Characterization of individual polynucleotide molecules using a membrane channel. Proc. Natl. Acad. Sci. 93, no. 24, pages 13770–13773.

[38] N. Kikuchi, C. M. Pooley, J. F. Ryder, and J. M. Yeomans. 2003. Transport coefficients of a mesoscopic fluid dynamics model. J. of Chem. Phys. 119, page 6388.

[39] R. Kimmich and N. Fatkullin. 2004. Advances in Polymer Science. Springer-Verlag, Berlin, 1-113 pages.

[40] James Kindt, Shelly Tzlil, Avinoam Ben-Shaul, and William M. Gelbart. 2001. DNA packaging and ejection forces in bacteriophage. Proc. Natl. Acad. Sci. 98, no. 24, pages 13671–13674.

[41] A. B Kolomeisky. 2008. How polymers translocate through pores: memory is important. Biophys. J. 94, page 1547.

[42] E. Kuusela. 2005. Steady-State Sedimentation of Non-Brownian Particles with Finite Reynolds Number. Otamedia Oy, Espoo.

[43] Esa Kuusela, Kai Höfler, and Stefan Schwarzer. 2001. Computation of particle settling speed and orientation distribution in suspensions of prolate spheroids. Journal of Engineering Mathematics 41, pages 221–235. 10.1023/A:1011900103361.

[44] L. D. Landau and E. M. Lifshitz. 1987. Fluid Mechanics. Butterworth-Heinemann, Oxford.

[45] Bin Li, Neal Madras, and Alan Sokal. 1995. Critical exponents, hyperscaling, and universal amplitude ratios for two- and three-dimensional self-avoiding walks. J Stat Phys 80, page 661.

[46] J. Li, M. Gershow, D. Stein, E. Brandin, and J. A. Golovchenko. 2003. DNA molecules and configurations in a solid-state nanopore microscope. Nature Materials 2, page 611.

[47] K. Luo, T. Ala-Nissila, and S.-C. Ying. 2006. Polymer translocation through a nanopore: A two-dimensional Monte Carlo study. J. of Chem. Phys. 124, page 034714.

[48] K. Luo, T. Ala-Nissila, S.-C. Ying, and A. Bhattacharya. 2007. Influence of Polymer-Pore Interactions on Translocation. Phys. Rev. Lett. 99, no. 14, page 148102.

[49] K. Luo, T. Ala-Nissila, S.-C. Ying, and R. Metzler. 2009. Driven polymer translocation through nanopores: Slow-vs.-fast dynamics. EPL (Europhysics Letters) 88, no. 6, page 68006.

[50] K. Luo, S. T. T. Ollila, I. Huopaniemi, T. Ala-Nissila, Pawel Pomorski, M. Karttunen, S.-C. Ying, and A. Bhattacharya. 2008. Dynamical scaling exponents for polymer translocation through a nanopore. Phys. Rev. E 78, no. 5, page 050901.

[51] N. Madras and G. Slade. 1996. The Self-Avoiding Walk. Birkhäuser, Boston.

[52] A. Malevanets and R. Kapral. 1999. Mesoscopic model for solvent dynamics. J. of Chem. Phys. 110, page 8605.

[53] A. Malevanets and R. Kapral. 2000. Solute molecular dynamics in a mesoscale solvent. J. Chem. Phys. 112, page 7260.

[54] A. Malevanets and R. Kapral. 2004. Mesoscopic Multi-particle Collision Model for Fluid Flow and Molecular Dynamics, In: *Lecture Notes in Physics* **640** ed. by M. Karttunen, I. Vattulainen, and A. Lukkarinen. Springer, Berlin, Heidelburg, 116-149 pages.

[55] S. Melchionna, M.G. Fyta, E. Kaxiras, and S. Succi. 2007. Exporing DNA translocation through a nanopore via a multiscale lattice-Boltzmann molecular-dynamics methodology. International Journal of Modern Physics C 18, page 685.

[56] Amit Meller. 2003. Dynamics of polynucleotide transport through nanometre-scale pores. Journal of Physics: Condensed Matter 15, no. 17, page R581.

[57] M. Muthukumar. 1999. Polymer translocation through a hole. J. of Chem. Phys. 111, pages 10371–4.

[58] Walter Neupert and Johannes M. Herrmann. 2007. Translocation of Proteins into Mitochondria. Annual Review of Biochemistry 76, no. 1, pages 723–749.

[59] N. T. Nguyen and S. T. Wereley. 2006. Fundamentals And Applications of Microfluidics, Second Edition (Integrated Microsystems). Artech House Publishers.

[60] J. Noonan. 1998. New Upper Bounds for the Connective Constants of Self-Avoiding Walks. J. Stat. Phys. 91, pages 871–888.

[61] D. Panja, G. T. Barkema, and R. C. Ball. 2007. J. Phys. Condens. Matter 19, page 432202.

[62] Debabrata Panja, Gerard T Barkema, and Robin C Ball. 2008. Polymer translocation out of planar confinements. Journal of Physics: Condensed Matter 20, no. 7, page 075101.

[63] O. Punkkinen. 2009. Conformations and Dynamics of Strongly Charged Biomolecules. Helsinki University of Technology. URL http://lib.tkk.fi/Diss/2009/isbn9789512299171/.

[64] S. Ramaswamy. 2001. Issues in the statistical mechanics of steady sedimentation. Advances in Physics 50, page 297.

[65] L. E. Reichl. 1998. A Modern Course in Statistical Physics. Wiley Interscience, New York.

[66] Katinka Ridderbos. 2002. The coarse-graining approach to statistical mechanics: how blissful is our ignorance? Studies In History and Philosophy of Science Part B: Studies In History and Philosophy of Modern Physics 33, no. 1, pages 65 – 77.

[67] M. Ripoll, K. Mussawisade, R. G. Winkler, and G. Gompper. 2004. Low-Reynolds-number hydrodynamics of complex fluids by multi-particle-collision dynamics. EPL (Europhysics Letters) 68, no. 1, page 106.

[68] Irwin Rubenstein and Sara B. Leighton. 1974. The influence of rotor speed on the sedimentation behavior in sucrose gradients of high molecular weight DNA's. Biophysical Chemistry 1, no. 4, pages 292 – 299.

[69] T. Sakaue. 2007. Nonequilibrium dynamics of polymer translocation and straightening. Phys. Rev. E 76, no. 2, page 021803.

[70] T. Sakaue. 2010. Sucking genes into pores: Insight into driven translocation. Phys. Rev. E 81, no. 4, page 041808.

[71] F. Sanger. 1949. The terminal peptides of insulin. Biochem J. 45(5), pages 563–574.

[72] F. Sanger and H. Tuppy. 1951. The amino-acid sequence in the phenylalanyl chain of insulin. 2. The investigation of peptides from enzymic hydrolysates. Biochem J. 49(4), pages 481–490.

[73] Alexis F. Sauer-Budge, Jacqueline A. Nyamwanda, David K. Lubensky, and Daniel Branton. 2003. Unzipping Kinetics of Double-Stranded DNA in a Nanopore. Phys. Rev. Lett. 90, no. 23, page 238101.

[74] Jonathan Schaffer. 2008. The Metaphysics of Causation. In: Edward N. Zalta (editor), The Stanford Encyclopedia of Philosophy. Fall 2008 edition.

[75] Xaver Schlagberger and Roland R. Netz. 2007. Anomalous Polymer Sedimentation Far from Equilibrium. Phys. Rev. Lett. 98, no. 12, page 128301.

[76] S. M. Simon, C. S. Peskin, and G. F. Oster. 1992. What drives the translocation of proteins? Proc. Natl. Acad. Sci. 89, page 3770.

[77] Gautam V. Soni and Amit Meller. 2007. Progress toward Ultrafast DNA Sequencing Using Solid-State Nanopores. Clin Chem 53, no. 11, pages 1996–2001.

[78] Todd M. Squires and Stephen R. Quake. 2005. Microfluidics: Fluid physics at the nanoliter scale. Rev. Mod. Phys. 77, no. 3, page 977.

[79] Arnold J. Storm, Cornelis Storm, Jianghua Chen, Henny Zandbergen, Jean-Francois Joanny, and Cees Dekker. 2005. Fast DNA Translocation through a Solid-State Nanopore. Nano Letters 5, no. 7, pages 1193–1197.

[80] W. Sung and P. J. Park. 1996. Polymer Translocation through a Pore in a Membrane. Phys. Rev. Lett. 77, no. 4, pages 783–786.

[81] H. N. V. Temperley. 1957. The Statistical Mechanics of the Steady State. Proc. Phys. Soc. B 70, page 577.

[82] B. Tinland, A. Pluen, J. Sturm, and G. Weill. 1997. Persistence Length of Single-Stranded DNA. Macromol. 30, page 5763.

[83] M. van der Laan *et al.* 2007. Motor-free mitochondrial presequence translocase drives membrane integration of preproteins. Nature Cell Biol. 9, page 1152.

[84] L. von Bertalanffy. 1968. General System Theory: Foundations, Development, Applications. George Braziller, New York.

[85] Nils Wiedemann, Ann E. Frazier, and Nikolaus Pfanner. 2004. The Protein Import Machinery of Mitochondria. Journal of Biological Chemistry 279, no. 15, pages 14473–14476.

[86] B. H. Zimm. 1956. Dynamics of Polymer Molecules in Dilute Solution: Viscoelasticity, Flow Birefringence and Dielectric Loss. J. Chem. Phys. 24, page 269.